NTNU – Trondheim
Norwegian University of
Science and Technology

Developing Force Control Scenarios on ABB IRB 4600 with Camera Capture of Dynamic Motions

Petter Kvernberg

Master of Science in Cybernetics and Robotics
Submission date: June 2015
Supervisor: Anton Shiriaev, ITK

Norwegian University of Science and Technology
Department of Engineering Cybernetics

Title: Developing Force Control Scenarios on ABB IRB 4600 with Camera Capture of Dynamic Motions.

Student: Petter Kvernberg.

Project description: The aim of the project is to plan, develop and analyze one complex scenario of robots that can be used in the future for different industries such as grinding and polishing of objects. The IRB 4600 robot will be used to develop scenarios where motions and dynamics will be studied. The focus of the thesis is to study the motions of the robot when it moves freely in space and when it is in contact with an object. To intersect with an object, force control (FC) is utilized. Measurements from the robot encoders will be compared to measurements from the camera system K-610 Series Optical CMM. After each run there will be performed improvements for the next experiment, possibly developing modifications and strategies to improve FC machining. It is expected that simulations followed by experiments will give an indication of the challenges and solutions surrounding the feasibility of the equipment for the specific study.

Thesis deadline: 8. June 2015.

Supervisor: Professor Anton Shiriaev.

Preface

This is the concluding Master thesis for the study program in Engineering Cybernetics at the *Norwegian University of Science and Technology* (NTNU). The work was carried out between January 2015 and June 2015. Experiences with robots from the project work at fall 2014 guided this project to develop and analyze complex scenarios.

The project gives motivation to continue working with robots and to give feasible solutions for different industries in the future. The reader of this thesis is expected to be superficially familiar with robot technology and engineering.

Trondheim - June 2015

Petter Kvernberg

Acknowledgment

I would like to thank Professor Anton Shiriaev for his valuable inputs and supervision during the project. I would also like to thank Postdoctoral Leonid Paramonov for assisting and for helping designing the tool used for FC. Then I would like to thank PhD Candidates Stepan Pchelkin and Sergey Kolyubin for giving guidance on the K-610 Series Optical CMM and the IRB 4600.

PK

Abstract

Finishing processes are among the earliest applications of industrial robots. Therefore, machining with the help of robot technology is widely used in industries today. The potential of increasing the efficiency and developing new complex tasks is still existing. This thesis investigate the scenarios by comparing the position of the end effector to a highly precise camera system. Thus, the physical behavior of the robot is always known compared to robot measurements itself.

The research is focused on two cases, which is the motion in free space and the motions while in contact with an object using *Force Control* (FC). Motions in free space are examined because it is desired to see the behavior of the end effector while no physical forces is applied. Afterwards we can compare if there exists similarities with the motions for a FC scenario. The FC scenario consist of a path while in contact with a leveled and planar metal object.

For the FC implementation, it was applied 1 to 50 Newton force towards a leveled object. The robot performed with a displacement for the end effector on the robot side up to 240 µm. The camera system measured the physical motion and revealed that each run between 1 and 50 Newton follows the same path, without displacement.

In the FC procedure, it was found through experimentation oscillations of 0.14 Hz along the path. These oscillations are existing for every FC scenario in this thesis. The oscillations should be compensated by a controller, which remains as future work. A suggestion is presented in the thesis which is about changing the velocity along the FC procedure from a constant c to a variable $h(x)$ as step based or as a polynomial. When a controller is developed, the research is one step closer for developing a quality strong product for a machining process by an industrial robot.

Sammendrag

Etterbehandlingsprosesser er blant de tidligste anvendelsene for industrielle roboter. Derfor er bruken av bearbeidingsprosesser av roboter brukt av mange bedrifter i dag. Potensiale for å forbedre effektiviteten og for å utvikle nye komplekse oppgaver finnes fortsatt. Denne oppgaven undersøker scenarioer ved å sammenlikne posisjoner fra enden av roboten med et meget presist kamerasystem. Da vet man alltid den fysiske oppførselen til roboten sammenliknet med robotens egne målinger.

Denne oppgaven undersøker bevegelser ved to tilfeller, som er ved bevegelser i fritt rom og bevegelser når roboten har kontakt med et objekt ved bruk av kraftkontroll (FC). Bevegelser i rommet er undersøkt, fordi man ønsker å se oppførselen roboten når den ikke er i fysisk kontakt med noe. Etterpå kan man sammenlikne og se om det er likheter med bevegelser for FC scenarioer. FC-banen består av en bane som berører et horisontalt metallobjekt.

For FC implementasjonen er det brukt 1 til 50 Newtons kraft mot et vannrett objekt. Da kunne man se en forskyving av tuppen av roboten fra robotens målinger på 240 µm. Kamerasystemet målte den fysiske bevegelsen og avslørte at hvert forsøk mellom 1 og 50 Newton følger samme bevegelse, uten forskyving.

I FC-prosedyren, ble det observert oscillasjoner på 0.14 Hz langs banen. Disse oscillasjonene er eksisterende for hvert eneste FC scenario. Det burde kompenseres for disse oscillasjonene ved å lage en kontroller, som forblir fremtidig arbeid. Et forslag er presentert i oppgaven som handler om å forandre hastigheten langs banen for FC-prosedyren fra en konstant c til en variabel $h(x)$ som er stegbasert eller som et polynom. Når kontrolleren er utviklet, er man et steg nærmere i å utvikle et kvalitetssikkert produkt for en behandlingsprosess av en industriell robot.

Contents

List of Figures

List of Tables

CHAPTER 1

Introduction

The history of modern robotics has many milestones within the last decades. Already in 1954, George Devol designed the first programmable robot, called the Programmed Article Transfer, Malone [10]. However, the applications of industrial robots did not explode before the 1970s and the 1980s. The first utilizations of finishing processes also arrived in this period, among these are Kazerooni and Her [8] and Mason [11]. The reason for researching robotics for finishing work was that manual machining of objects tend to be tiresome and monotonous. There is also a strain of injuries to humans due the repetitiveness work, Zhang et al. [23].

To perform finishing work with an industrial robot, it must complete controlled motions of interaction between itself and its environment, Siciliano and Villani [19]. In order to establish control, *Force Control* (FC) is applied, where force and torque are part of the feedback control loops, Kroeger [9]. Thus, it can be accomplished finishing processes such as grinding and polishing of objects with high amount of repetitiveness ability.

Successful execution of an interaction task with the surroundings requires accurate planning, such that both the robot and the environmental objects remains unharmed. If there exists planning errors, a contact force may cause deviation of the end effector from the desired trajectory, Siciliano and Villani [19]. The combination of object stiffness and the position control accuracy give raise to such deviation.

This thesis will examine such a scenario, where FC is applied to an environmental object. The performance will be examined by comparing the position of the end effector with a camera system called the K-610 Series Optical CMM produced by

Nikon Metrology. Thus, the camera system will reveal the physical behavior from the robot measurements itself. By discovering inaccuracy of the robot position, the thesis will recommend feasible solutions to improve quality of interaction from analysis of force and position measurements.

1.1 Motivation

The reason why the research of robots is important is the possibility of creating solutions, which are improving the efficiency of industrial processes. By applying robots, it provide the opportunity to replace operators, which release them from monotonous work and quality of products can become more robust.

One such industry is production of guitars, which is a delicate process from start to end, requiring robots for the polishing part of the production. The final polishing of the guitars however, still requires the touch of humans to obtain a satisfied product, *The Music Zoo* [22]. The fact that not every part of a industrial process is not done by robots yet, give motivation for this thesis.

The challenge is to achieve a behavior of the robot, which can perform high precision motions. Such performance can be found by investigating possible solutions, by e.g. changing the tool design, optimizing robot paths or creating controllers which will compensate for unwanted behaviors such as deviation in position from planned trajectory, these are future themes discussed by Chen and Dong [6].

Since the industry such as polishing of guitars and other part removal manufacturers are eager after feasible and complex robot solutions, it is required to develop robots, which can execute new tasks with high accuracy. Furthermore, since this thesis investigate behaviors of the robot by comparing it to a highly precise camera system, the thesis can be used as background and source for developing new solutions and research questions.

1.2 Objectives

The thesis will plan, perform and analyze two cases when using the IRB 4600 and the K-610 Series Optical CMM. Both aspects deals with the position comparison between the robot and camera system.

The first component is to compare the positions without intersecting with environmental objects, given in Chapter 4. The goal is to study and experience how the camera system behave with respect to robot measurements. The scenario will provide possibilities of comparing trajectories when applying FC in the second case.

The second experiment, intersection with an object will be executed by utilizing FC, given in Chapter 5. A tool will be designed to perform such a scenario where both forces and positions will be measured.

The thesis performs a numerous experiments and analyzing of measurements. The final goal is to discover a response of undesired behavior such as deviation in position when applying FC, such that the thesis can provide feasible solutions. A solution can be a compensation in the performance of the trajectory. The camera system is an extra source of information, which can reveal dynamics by comparing position of the robot at every time step by visualizing physical movements.

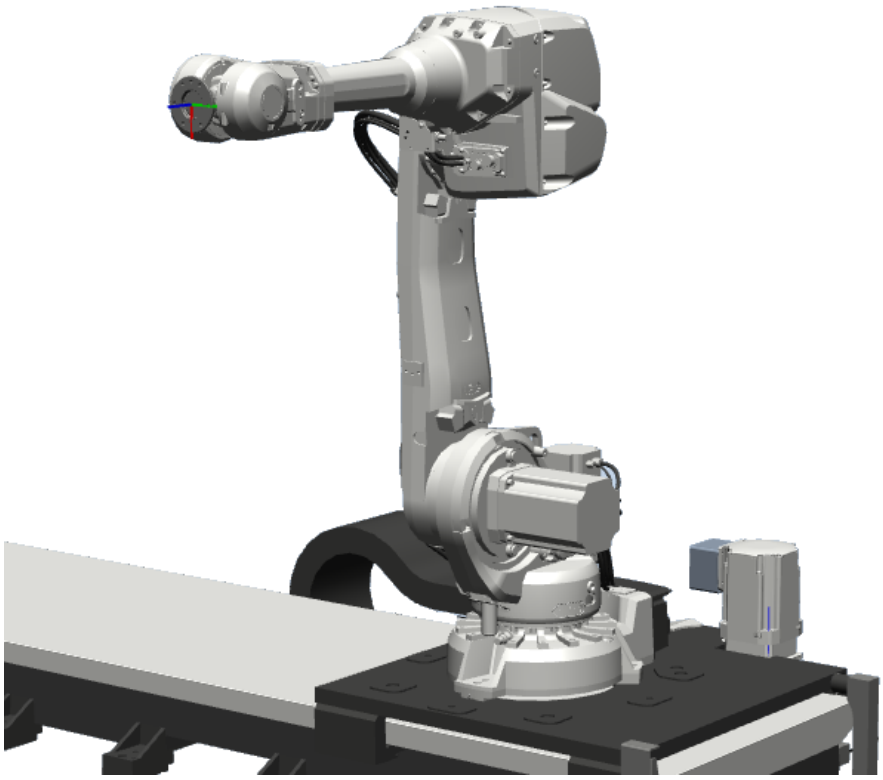

Figure 1.1: Model of the IRB 4600 on track viewed from RobotStudio.

1.3 Contribution

The contribution in this thesis is provided in the results presented from the developed experiments and the experiences achieved during the process. The difference from this thesis from much other research, is the continuous comparison between the camera system and the robot when applying FC.

Because of two measurement sources, it is possible to provide if the robot determine it is in the correct position. The thesis will at the end contribute by proposing possible solutions of compensations for deviation in the position reasoned by the presented results.

1.4 Structure of the Report

This text is organized into six chapters where acronyms are supported in the Appendices and basics of MATLAB and Rapid code and relevant manuals are attached as a digital file. The structure of the concluding report is specified as follows.

Chapter 1 is an introduction to the report where motivation for the work, objectives and contributions are clarified.

Chapter 2 presents basic theory the reader should be known to before proceeding through the report.

Chapter 3 is a detailed account of modeling of the IRB 4600 and a description of how the camera system works and how to make it functional with the robot.

Chapter 4 deals with the first experiment, where trajectories without FC are examined. This will also give an indications of how to proceed with FC experiments in Chapter 5 because of experience with the camera system.

Chapter 5 builds further on experiences done in Chapter 4 and take complexity to a new level. The experiments in this chapter investigate the reactions when utilizing FC and applying it to a chosen object.

Chapter 6 give a conclusion of the whole text and summarize contributions of achievements. There will also be given recommendation of further work about the camera and robot system.

CHAPTER 2

Mathematical Preliminaries

This chapter briefly explains theory included in this thesis. The first aspect is to study forward and inverse kinematics, which are used to derive the IRB 4600 model in section 3.1. Afterwards, relevant signal processing theory will presented. Signals that are measured from the robot and the camera require analysis and processing to see characteristic behaviors.

2.1 Robot Kinematics

This section will look at the relationship between joint variables q_i and the position and orientation of the device at the robot wrist. Any device installed on the robot wrist, is defined as an end effector, Robotiq [18]. At first, the forward kinematics will be considered, which calculates the position of the end effector and orientation by using the values for each joint. Afterwards, the inverse kinematics will be presented, which determines the values of each joint variable given the position of the end effector.

2.1.1 Forward Kinematics

Forward kinematics describes the relation between each joint of a robot manipulator. The i^{th} position and orientation of the robot are applied in a homogeneous transformation matrix A_i. This matrix represents a product of four quantities θ_i, a_i, d_i and α_i, which can be seen in equation 2.1. The application of equation 2.1 is reffered to in robotics as the *Denavit-Hartenberg* (DH) convention, Fiene [7].

$$A_i = \text{Rot}_{z,\theta_i}\text{Trans}_{z,d_i}\text{Trans}_{x,a_i}\text{Rot}_{x,\alpha_i} \tag{2.1}$$

The matrix A_i varies as the configuration of the robot is changed, where position and orientation are derived at every time step. Since all joints for an IRB 4600 are only rotational, A_i is only a function of a single joint variable, namely q_i. This means that the DH convention can be written as $A_i = A_i(q_i)$. By applying basic homogeneous transformations, equation 2.1 can be represented as equation 2.2.

$$A_i = \begin{bmatrix} \cos(\theta_i) & -\sin(\theta_i)\cos(\alpha_i) & \sin(\theta_i)\sin(\alpha_i) & a_i\cos(\theta_i) \\ \sin(\theta_i) & \cos(\theta_i)\cos(\alpha_i) & -\cos(\theta_i)\sin(\alpha_i) & a_i\sin(\theta_i) \\ 0 & \sin(\alpha_i) & \cos(\alpha_i) & d_i \\ 0 & 0 & 0 & 1 \end{bmatrix}, \tag{2.2}$$

Robotiq [18].

Equation 2.2 shows the derivation of equation 2.1 which has the total rotation in the 3×3 upper left corner and the total length in the 3×1 upper right corner. The representation of total transformation and rotation from $A_1 \dots A_n$ is called the transformation matrix, and is denoted by T_n^0. For the end effector, the position and orientation can therefore be written as equation 2.3, adapted from Spong et al. [20, p. 76].

$$H = T_n^0 = A_1 \dots A_n = \begin{bmatrix} R_n^0 & o_n^0 \\ 0 & 1 \end{bmatrix} \tag{2.3}$$

To derive the forward kinematics for n joints of a robot, the method is to follow an algorithm given in Spong et al. [20, p. 110]. The procedure consists of nine steps, starting by locating and labeling the joint axes $z_0, \dots, z_{n-1}$, and finishing by forming the T_n^0 transformation matrix. By following the nine steps, the expression become as presented in equation 2.3, describing every frame from o_0 to o_n. In other words, the position and the orientation of the end effector can be expressed from the base coordinates.

2.1.2 Inverse Kinematics

Inverse kinematics deals with the opposite of forward kinematics. Instead of determining the position and orientation of the end effector in terms of the joint variables, the joint variables are solved in terms of the position and orientation

of the end effector. Deriving the inverse kinematic problem introduce more problems of complexity than forward kinematics. The problem is to find a solution, or possibly multiple solutions of the equation

$$T_n^0(q_1, \ldots, q_n) = H \tag{2.4}$$

where H is the desired position and orientation of the end effector. The inverse kinematic problem is to determine the joint variables such that equation 2.4 is solved. For a robot with six joints, it is possible to decouple the problem if the last three joints are intersecting at a point. These two problems are known as inverse position kinematics and inverse orientation kinematics. The procedure of the determination is described in details in Spong et al. [20, p. 93]. The summarized procedure for a six DOF robot is given by the following steps:

Step 1: Determine $q1, q2, q3$ such that the wrist center has coordinates given by

$$o_c^0 = o - d_6 R \begin{bmatrix} 0 & 0 & 1 \end{bmatrix}^T \tag{2.5}$$

Step 2: Use the joint variables in Step 1 to calculate R_3^0

Step 3: Find a set of Euler angles corresponding to the rotation matrix

$$R_6^3 = (R_3^0)^{-1} R = (R_3^0)^T R \tag{2.6}$$

where R is given and R_3^0 can be calculated once the first three joint variables are known.

2.2 Signal Processing

This section review elements that are central in signal processing. First, an inspection of the Butterworth Filters will be presented, which is characterized to have a flat response until the cut-off frequency. Afterwards it will be considered ways of processing a signal by looking into the Fourier Series, Power Density Spectrum and Cross Correlation.

2.2.1 Butterworth Filters

The Butterworth filter is a filter that is designed to have no ripples from 0 Hz until the cut-off frequency. Because of a flat response until the cut-off frequency, the Butterworth filter has a wide transition band as the filter changes from pass band to stop band. The ideal frequency response is referred to as a brick wall filter, which can be seen in figure 2.1. The figure also illustrates the steepness for different orders of the filter, whereas it decrease the gain with 20 Db/decade for every n^{th} order of the filter.

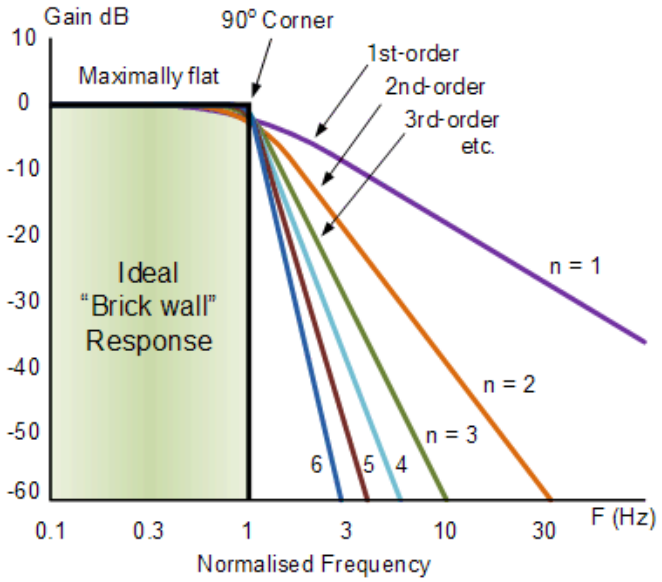

Figure 2.1: Frequency response for a Butterworth filter adapted from Storr [21], where n is the chosen filter order.

The following lowpass Butterworth filter equation is taken from *Digital Signal Processing* by Proakis and Manolakis [17], and are characterized by the magnitude-squared frequency response in equation 2.7.

$$|H(\Omega)|^2 = \frac{1}{1 + (\Omega/\Omega_c)^{2N}} = \frac{1}{1 + \epsilon^2(\Omega/\Omega_p)^{2N}}, \tag{2.7}$$

where Ω_c is the cut-off frequency at -3 dB, Ω is equal to $2\pi f$, N is the filter order, Ω_p is the passband edge frequency, and $1/(1+\epsilon^2)$ is the band-edge value of $|H(\Omega)|^2$.

2.2.2 Fourier Series

The Fourier series are a mathematical representation of a periodic signal, which is a linear weighted sum of harmonically related sinusoids or complex exponentials. For a periodic discrete-time periodic signal $x(n)$ with period N, the following expression applies for the Fourier series,

$$x(n) = \sum_{k=0}^{N-1} c_k e^{j2\pi kn/N}, \tag{2.8}$$

where c_k are the coefficients in the series representation. Equation 2.8 is often called the Synthesis equation, or the *Discrete-Time Fourier Series* (DTFS). In terms of finding the desired expression for the Fourier coefficients of the signal $x(n)$, it is given

$$c_k = \frac{1}{N} \sum_{n=0}^{N-1} x(n) e^{-j2\pi kn/N}, \tag{2.9}$$

which is known as the Analysis equation. For further explanations of the Fourier series review *Digital Signal Processing* by Proakis and Manolakis [17].

2.2.3 Power Density Spectrum

In order to understand where to cut frequencies when designing low pass filters or to compare the power of different signals, it is central to study the strength of a signal in the frequency domain relative to other signals. For a periodic signal, there exists infinite energy and finite power average power, given as

$$P_x = \frac{1}{T_p} \int_{T_p} |x(t)|^2 dt. \tag{2.10}$$

The frequency analysis of continuous-time periodic signals is given by the Synthesis equation as

$$x(t) = \sum_{k=-\infty}^{\infty} c_k e^{j2\pi F_0 t}, \tag{2.11}$$

where c_k is the complex conjugated and F_0 determines the fundamental frequency, $F_0 = 1/T_p$. By further deriving the complex conjugate of the Synthesis equation (2.11) and substitute for $x(t)$ in equation 2.10, the following is obtain, adapted

from Proakis and Manolakis [17],

$$P_x = \frac{1}{T_p} \int_{T_p} x(t) \sum_{k=-\infty}^{\infty} c_k^* e^{j2\pi F_0 t} \tag{2.12}$$

$$= \sum_{k=-\infty}^{\infty} c_k^* \left[\frac{1}{T_p} \int_{T_p} x(t) e^{j2\pi F_0 t} \right] \tag{2.13}$$

$$= \sum_{k=-\infty}^{\infty} |c_k|^2. \tag{2.14}$$

It is then stated a relation between the power signals, and it gives further the *Parsecal's relation* for power signals as

$$P_x = \frac{1}{T_p} \int_{T_p} |x(t)|^2 dt = \sum_{k=\infty}^{\infty} |c_k|^2. \tag{2.15}$$

To illustrate the power of signals, notice the *Power Density Spectrum* (PDS) in figure 2.2, which only consist of a single complex exponential. For further explanations of the power density spectrum, study *Digital Signal Processing* by Proakis and Manolakis [17].

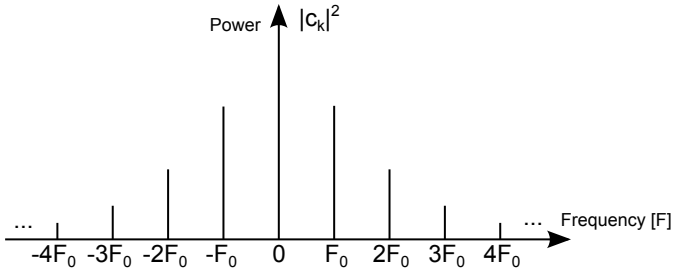

Figure 2.2: Power density spectrum of a periodic signal, the figure is adapted from *Digital Signal Processing* by Proakis and Manolakis [17].

2.2.4 Cross Correlation

The cross correlation defines how well two signals correlate to each other. The output is given as energy of the signals and tell how they match. Then the lag can be calculated, and to further compare the signals by adjusting for the lag in one

signal. For two signals $x(n)$ and $y(n)$, the cross correlation is defined as

$$r_{xy}(l) = \sum_{n=-\infty}^{\infty} x(n)y(n-l), \qquad l = 0, \pm 1, \pm 2, \ldots \tag{2.16}$$

where l is the lag parameter. For further explanations of the cross correlation review *Digital Signal Processing* by Proakis and Manolakis [17].

This chapter has provided theory to understand signal processing throughout the thesis and kinematics of the modeling in Chapter 3. Further, the next chapter will focus on kinematics specially for the IRB 4600 and calibration of the K-610 Series Optical CMM.

CHAPTER 3

Modeling and Calibration

This chapter is divided into two elements, where the work consist of the application of two different systems, the IRB 4600 and the K-610 Series Optical CMM. Firstly, the kinematics of the IRB 4600 will be derived in section 3.1, where the methods and concepts from section 2.1 will be used and applied to the IRB 4600. Secondly, the methods used for calibrating the K-610 Series Optical CMM will be elaborated. In order to utilize the Optical CMM, it is required to calibrate with optimal precision. It is also required to have a procedure of how the device is calibrated and adapted to the case study in the laboratory. This is described in details in section 3.2.

3.1 IRB 4600 Modeling

The IRB 4600 consists of six links connected together by joints. All six joints are rotational, causing the calculations to become more complex than if there were perpendicular joints. By using theory stated in section 2.1, the solutions for the forward and inverse kinematics for the IRB 4600 can be derived. Specifications of the IRB 4600 can be found in the Appendices, *IRB 4600 Industrial Robot*.

3.1.1 Forward Kinematics

As stated in section 2.1.1, the forward kinematics let us derive the position and orientation of the end effector by using the values of each joint of the IRB 4600. Each joint is calculated using trigonometrical symmetries and properties. By proceeding with systematical derivations, the position of the end effector is found by calculating joint q_1 to q_6. Kinematics analysis of the 6-linked robot is complex,

but by using techniques as the DH convention described in section 2.1.1, the analysis is simplified. By utilizing DH convention, the derivations can be understood universally and is more accepted for other engineers, Spong et al. [20].

Each joint q_i of the robot, are assigned an unique frame. As DH convention is utilized to define frames, the following two features must also be satisfied to use equation 2.1 and find unique numbers for a, d, θ and α.

(DH 1) The axis x_1 is perpendicular to the axis z_0.

(DH 2) The axis x_1 intersects the axis z_0.

Spong et al. [20, p. 78].

By using the constraints (DH1) and (DH2), and by defining the first frame to the origin $x_0y_0z_0$ as shown in figure 3.1, the DH convention can be used to calculate the position and orientation of the end effector.

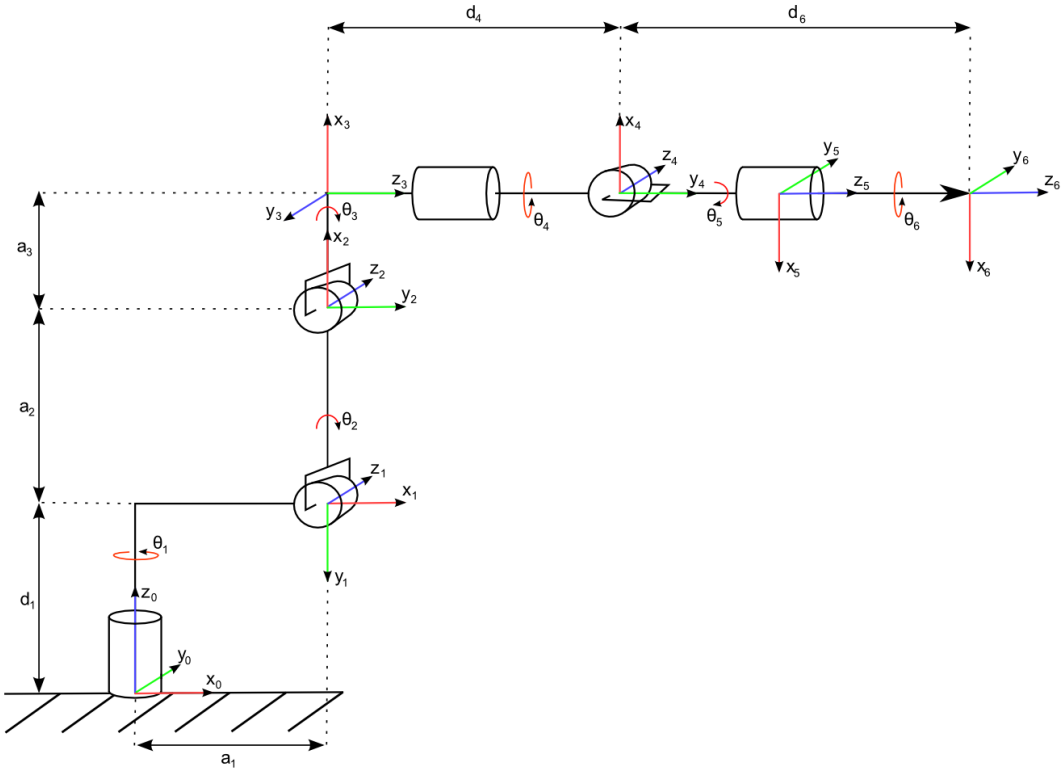

Figure 3.1: DH coordinate frame assignment for the IRB 4600. Each frame is rotated and translated with respect to table 3.1

In table 3.1, each link are assigned values and variables related to figure 3.1. The values a_i, d_i, θ_i and α_i in table 3.1 are then calculated by the DH convention represented in equation 2.2. Thus, T_6^0 can be presented, declaring the position of the end effector by multiplying every basic homogeneous transformation as

$$H = T_6^0 = A_1 \dots A_6 = \begin{bmatrix} R_6^0 & o_6^0 \\ 0 & 1 \end{bmatrix} \tag{3.1}$$

The variables d_i and a_i are known lengths of the IRB 4600, given in table 3.2. The joint variable α_i is also known by the frame assignment in figure 3.1 and is given in table 3.1.

Link	$\boldsymbol{\theta_i}$	$\boldsymbol{d_i}$	$\boldsymbol{a_i}$	$\boldsymbol{\alpha_i}$
1	θ_1	d_1	a_1	$-\frac{\pi}{2}$
2	$\theta_2 - \frac{\pi}{2}$	0	a_2	0
3	θ_3	0	a_3	$-\frac{\pi}{2}$
4	θ_4	d_4	0	$\frac{\pi}{2}$
5	$\theta_5 + \pi$	0	0	$\frac{\pi}{2}$
6	θ_6	d_6	0	0

Table 3.1: DH parameters for the IRB 4600.

Variabel	**Value [m]**
d_1	0.495
d_4	0.960
d_6	0.135
a_1	0.175
a_2	0.900
a_3	0.175

Table 3.2: Known lengths from product manual ABB [2], data sheet is also supplemented in Appendices *IRB 4600 Industrial Robot*.

The last variable including in equation 3.1 is θ_i, which is given by the current position of each joint of the robot. The thesis vary between using o_6 as last coordinate frame and o_7, since the frames move similarly, the choice is arbitrary because o_6 and o_7 is calculated by the same number of joint variables. In other

words, the frame o_7 is defined by applying a rotation and translation towards a point from o_6. The numerical calculations of the forward kinematics are attached as a digital file.

3.1.2 Inverse Kinematics

In this section, the inverse kinematics will be derived for the IRB 4600. The calculations builds on theory presented in section 2.1.2. The procedure of calculations will be, to first find the position of the intersection of the wrist center, and then find the orientation of the wrist using Euler angles. The first variable θ_1 is calculated straight forward from figure 3.2a, then it can be seen from the figure that the following yields

$$\theta_1 = \text{Atan2}(y_c, x_c), \tag{3.2}$$

where $\text{Atan2}(y_c, x_c)$ is the two argument arctangent function defined for all $(x, y) \neq (0, 0)$. When calculating θ_2 and θ_3 for the robot, θ_1 is given and figure 3.2b can be considered.

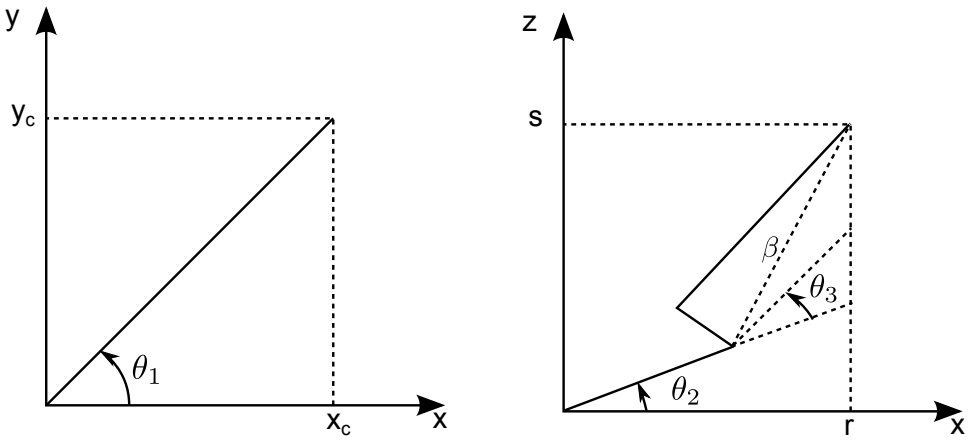

(a) Finding θ_1.

(b) Finding θ_2 and θ_3.

Figure 3.2: Projecting onto the plane formed by θ_1, θ_2 and θ_3.

Because of the robot specifications observed from figure 3.2, the elbow with an offset need to be dealt with, which give raise for a more complex calculation of θ_2 and θ_3. Moreover, since the motion of the second and third links is planar, the

joints can be calculated by the law of cosines as

$$\theta_3 = \text{Atan2}(\sqrt{1 - D^2}, D) - \frac{\pi}{2} + \text{Atan2}(a_3, d_4), \tag{3.3}$$

where

$$D = \frac{r^2 + s^2 - a_2^2 - \beta^2}{2a_2\beta}, \tag{3.4}$$

$$s = z - d_1, \tag{3.5}$$

$$r = \sqrt{(x - a_1)\cos(\theta_1))^2 + (y - a_1)\sin(\theta_1))^2}), \tag{3.6}$$

$$\beta = \sqrt{a_3^2 + d_4^2}. \tag{3.7}$$

Similarly as θ_3, θ_2 is calculated as

$$\begin{aligned}\theta_2 = &- \text{Atan2}(s, r) + \text{Atan2}(\beta \sin(-\theta_3 - \frac{\pi}{2} + \text{Atan2}(a_3, d_4)), a_2 \\ &+ \beta \cos(-\theta_3 - \frac{\pi}{2} + \text{Atan2}(a_3, d_4))) + \frac{\pi}{2}.\end{aligned} \tag{3.8}$$

The three final joint variables correspond to a given position of the wrist center given by the frame $x_3y_3z_3$. In order to find the solution of the final joint variables, Euler angles is used, which correspond to a given matrix R given as

$$R = R_{z,\phi}R_{y,\theta}R_{z,\psi} = \begin{bmatrix} c\phi c\theta c\psi - s\phi s\psi & -c\phi c\theta s\psi - s\phi c\psi & c\phi s\theta \\ s\phi c\theta c\psi + c\phi s\psi & -s\phi c\theta s\psi + c\phi c\psi & s\phi s\theta \\ -s\theta c\psi & s\theta s\psi & c\theta \end{bmatrix}, \tag{3.9}$$

Spong et al. [20, p. 54], where

$$\theta_4 = \phi, \tag{3.10}$$

$$\theta_5 = \theta, \tag{3.11}$$

$$\theta_6 = \psi. \tag{3.12}$$

From the first three joints, the following rotation around the wrist center is obtained,

$$R_3^0 = \begin{bmatrix} r_{11} & r_{12} & r_{13} \\ r_{21} & r_{22} & r_{23} \\ r_{31} & r_{32} & r_{33} \end{bmatrix}. \tag{3.13}$$

By comparing equation 3.9 and 3.13, θ_5 is obtained as

$$\theta_5 = -\text{Atan}(2\sqrt{r_{13}^2 + r_{23}^2}, r_{33}). \tag{3.14}$$

If the square root in equation 3.14 is positive, θ_4 and θ_6 are obtained as the following

$$\theta_4 = \text{Atan2}(r_{23}, r_{13}), \tag{3.15}$$

$$\theta_6 = \text{Atan2}(r_{32}, -r_{31}) - \pi. \tag{3.16}$$

The summarized achievement is then a solution for each joint θ_1 to θ_6, given a position $x_6 y_6 z_6$. The numerical calculations are supported in a digital file attached to this thesis.

3.1.3 IRB 4600 Gear Ratio

From the encoders of the robot joints, the output is given as numerical values of the joints, which has deviations from the correct values. The output does not include the gear ratio of the robot. Thus, the gear ratio must be included by multiplying it with the joint variables as followed:

$$g = \begin{bmatrix} g_{11} & 0 & 0 & 0 & 0 & 0 \\ 0 & g_{22} & 0 & 0 & 0 & 0 \\ 0 & 0 & g_{33} & g_{34} & 0 & 0 \\ 0 & 0 & 0 & g_{44} & 0 & 0 \\ 0 & 0 & 0 & g_{54} & g_{55} & 0 \\ 0 & 0 & 0 & g_{64} & g_{65} & g_{66} \end{bmatrix}, \tag{3.17}$$

where

$$
\begin{aligned}
g_{11} &= -\,125.070999, & g_{22} &= 171.000000,\\
g_{33} &= 142.929001, & g_{44} &= -\,60.000000,\\
g_{55} &= 66.894699, & g_{66} &= -\,50.000000,\\
g_{34} &= 0.000000, & g_{54} &= -\,(-5.000000),\\
g_{65} &= -\,28.000000, & g_{64} &= -\,(-3.000000).
\end{aligned}
$$

The joint angles can then be found by using the matrix in equation 3.17 to calculate equation 3.18.

$$q(t) = \mathrm{inv}(g) \begin{bmatrix} q_1 & q_2 & q_3 & q_4 & q_5 & q_6 \end{bmatrix}^T. \tag{3.18}$$

By deriving equation 3.18, the forward kinematic problem can be solved in order to find the coordinates of the end effector with respect to the joint angles.

3.2 K-610 Series Optical CMM

The K-610 Optical CMM is a high precision camera system, which operate as a third party instrument tracking system. The motions of the robot can be tracked in real time by the Optical CMM which increase robotized inspections for manufacturing tasks, *K-Series Optical CMM* Nikon [12]. To generate purpose of the Optical CMM, the system must be calibrated such that measurements are valuable for comparison with robot measurements.

The process of calibration is a straightforward operation. However, it requires high amount of precision with the measurement device, called a Space Probe, to achieve a satisfactory results. The Space Probe measure multiple points in the space to define frames, which can be related to *Light Emitted Diodes* (LED)s physical placements on the robot base and tool.

The goal of the procedure is to define two frames, which relates to the robot base and tool device frame. A minor fault in a measurement situation will give offset between the camera and the robot, such that the correspondence is inoperative and unscientific.

One way of compensating for the measurements, is to adjust the frames after the measurement situation, but this is a challenging procedure in order to achieve less deviation. The most important matter is to have objects, which are located leveled with respect to the robot. By achieving horizontal measurements, the procedure of adjustments is decreased. Finding horizontal objects is however, challenging to find and achieve, especially for the entire reachability of the robot. Since the procedure of defining frames is challenging, the following sections will attempt to describe this method of calibrating the Optical CMM in details. First, a description of the integrated equipment will be elaborated.

3.2.1 Optical CMM Facilities

The camera system utilized in the experiments are as mentioned initially of this section the K-610 model of the Optical CMM. The camera itself consist of three lenses, where each lens track all the LEDs to visualize in 3D perspective with optimized precision. Measurements of the K-610 has the capacity of analyzing a volume of 17 m^3, from a distance of 1600 mm up to 6000 mm, whereas the volumetric accuracy can reach up to 60 µm.

Compared to the other models for the K-Series, the K-610 is most accurate, see the manual *K-Series Optical CMM solutions* [14] for more specifications. The Optical CMM is used to measure LEDs position related to itself.

The LEDs are attached to static equipment or objects which are desired to track, described more in section 3.2.3. The measured volume has a form of a pyramid, illustrated in figure 3.3 where the K-600 depicted, has the same volume measurement as the K-610. For a LED to be visible, the Optical CMM must have a straight line of sight towards the LED inside the limited volume. If a LED appears outside the volume, the data from these measurements will vanish.

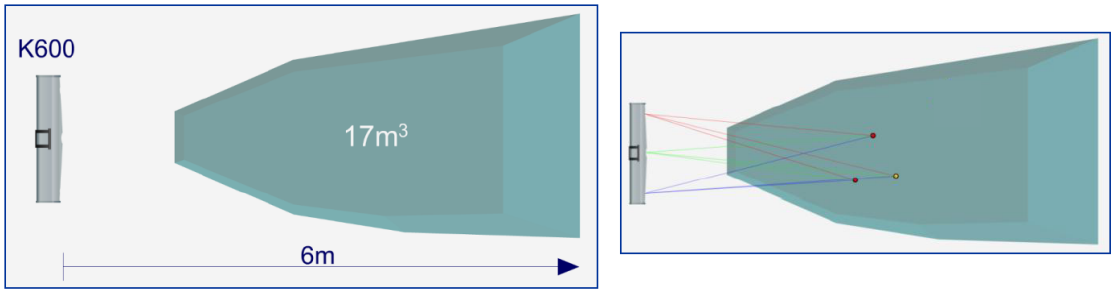

Figure 3.3: Measurement volume for the K-600 series, whereas the K-610 series is also specified with the same measurement volume depicted, *K-Series Training* [15].

A controller is used to connect all the components for the K-series system. LEDs are attached through Strober units, and the controller make sure the information from the measurements are synchronized at each time step. The synchronized signal is then sent via an Ethernet port to a PC for data capture and analysis. The sampling frequency of the Optical CMM can reach 100 Hz, which is slower than the robot encoders sampling time of approximately 250 Hz. The entire connection setup is illustrated in figure 3.4. For further details about the setup, see the manual *K-Series Training* [15]. The manual also describe how to use every software needed to successfully receive data from the procedure.

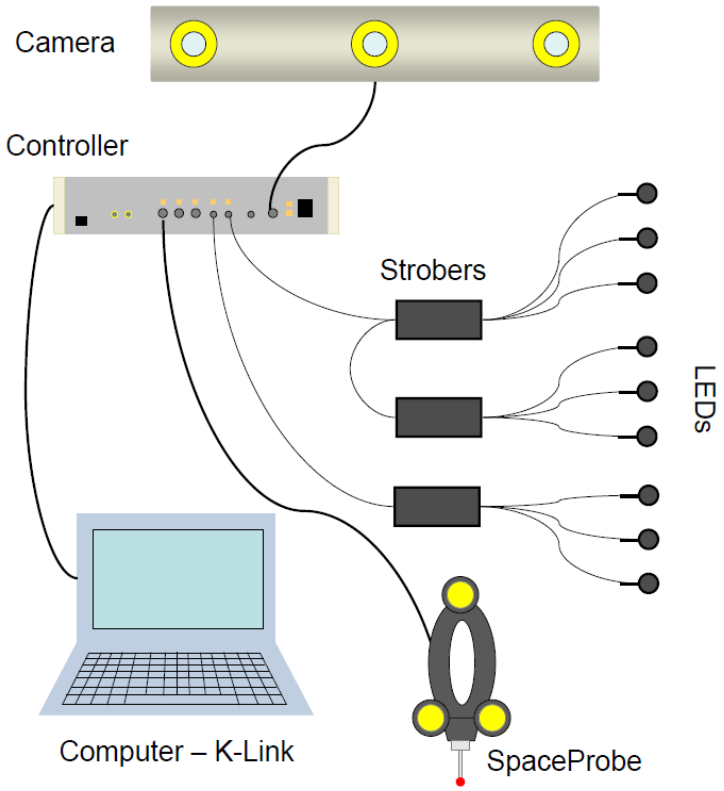

Figure 3.4: Connection setup for the K-610 Series, *K-Series Training* [15].

3.2.2 Calibration of Measurement Devices

In order to achieve satisfactory precision, it is first required to calibrate the measurement devices. There are two devices that are committed to be calibrated, which is the Space Probe and the K-Ref bar. The Space probe must be calibrated because it is the device that is used to measure points on physical objects in order to define frames. Frame definition will be described in section 3.2.4.

Without calibration of the Space Probe, the position of the tip of the probe cannot be related to its LEDs. In order to improve performance for the orientation and position for the camera measurements, the K-Ref bar also needs to be calibrated. It is a bar, which has built in LEDs, similarly as the Space Probe with other dimensions. The K-Ref bar is held in different positions and orientations in front of the Optical CMM to be calibrated.

The procedure consists of 23 positions to calibrate the K-Ref bar and at least eight measurements to calibrate the Space Probe. To view the procedure of the calibration, see *K-Series Training* [15]. After calibration, it is shown an error for both devices, where the goal is to minimize the deviation from the reference.

For the Space Probe to be satisfactory calibrated, an error of 0.04 mm is required. For the K-Ref bar, there are requirements for each individual position and orientation within 0.10 mm. The Space Probe calibration can be seen in figure 3.5. The red lights indicates each LED on the Space Probe, which turn green if they are visible. For the calibration to be adequate and valuable, the Space Probe must be measured consisting of rotations of 132° longitudinal and 156° sideways with the mentioned deviation of 0.04 mm.

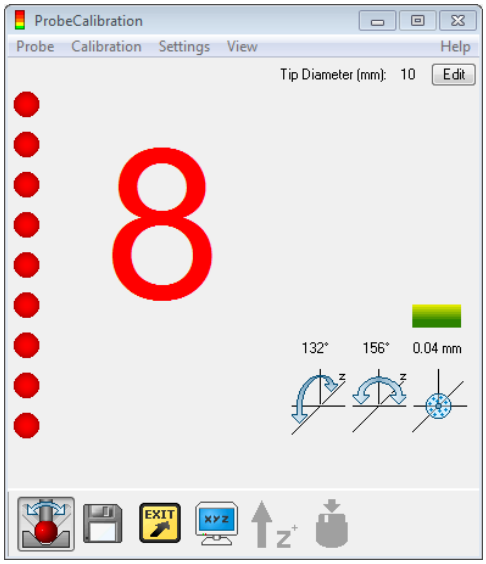

Figure 3.5: Calibration result of the Space Probe which satisfies 0.04 mm. The calibration is obtained for every test scenario in the thesis.

3.2.3 LED Placement

To define frames in section 3.2.4, LEDs needs to be placed both in the robot tool and the robot base. Then the LEDs placed at the base can relate to position and orientation of the tool such that we can track the position, and later compare it to the robot. To attach LEDs it requires preconditions, these are conditions to place

the LEDs correctly with respect to the Optical CMM. For detailed considerations of the LED placements, see the manual *LED Placement Guide* [16]. The LED placement done for one of the experiments in chapter 4 is shown in figure 3.6. Here we have the LEDs placed on the robot base in figure 3.6a and the robot tool in figure 3.6b.

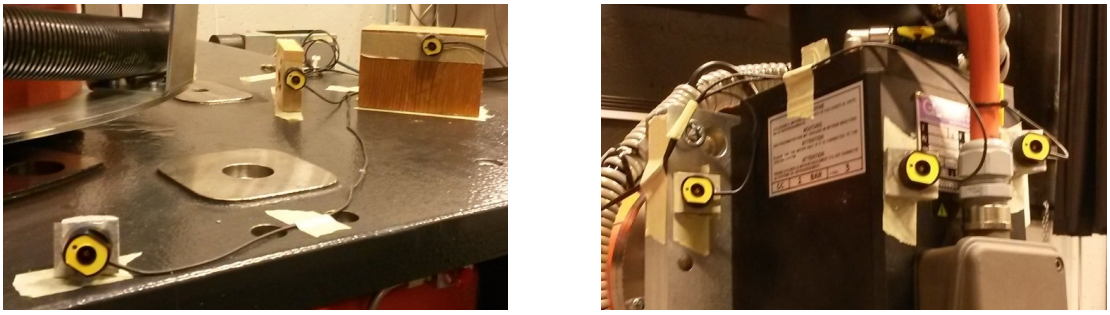

(a) LEDs on robot base.

(b) LEDs on robot tool.

Figure 3.6: LED placement on the robot. The locations are focused to have variation in depth and width.

The LEDs are placed with significant spread, pointing directly at the Optical CMM for all situations. When LEDs are attached to moving objects, like the end effector, both the motion and the placement must be considered to have a straight line of sight to the LEDs at all time. Possessing direct contact between the LEDs and the Optical CMM is necessary to acquire all data from the simulation situation.

The LEDs are also placed with different height and depth with respect to the Optical CMM as seen in figure 3.6. This will make it easier to define and to track the frames created by the placement of the LEDs without amplified noise components. It is sufficient that one LED deviate from the rest with respect to height and depth of the placement. Two LEDs can be placed at the same height or depth without achieving unscientific results when using only three LEDs to define a frame.

3.2.4 Defining Frames

When LEDs are attached to the robot base and tool, frames can be defined, which relates to the position and orientation of the LEDs. It is required to include at least three LEDs to define a frame. Nikon Metrology supplies with the software Geoloc, which lets the user relate frames to LEDs.

In order to define the frames, the position of the LEDs must be used and it must be created a specific amount of objects. These objects are defined by using the Space Probe. The shape of the objects defines where the axes are aligned, e.g. a circle would define a normal from its origin. To define an entire frame, several objects must be combined. The objects defined in the experiments in this thesis are:

- Cylinder: Defines the z axis, the x, y plane and the origin of the frame. The cylinder can be replaced by defining a plane and a circle, individually.
- Line: Defines the x axis, completing the frame.

In order to define frames that are orientated horizontally with the robot axes, it is important to use the Space Probe on objects which are leveled with the robot levels. Since both the tool and the base will be moved under trajectory execution, the frames must be dynamic. Dynamic frames means that the Optical CMM will track the position of the LEDs and map it to the frame related to the base LEDs.

Creating dynamic frames are necessary in order to achieve a real time comparison between the Optical CMM and the robot. Further explanations of the the Geoloc software is found in the manual *K-Series Training* [15], while details of creating frames in Geoloc can be found in the manual *Introduction to Frames* [13].

The procedure of defining frames consist of several steps that should be followed precisely in order to obtain meaningful results. Then the comparison between the camera and the robot measurements can be accomplished. The comparison between the camera and the robot are performed by comparing LEDs with values given by the robot encoders.

The base is the simplest, whereas the LEDs on the base are compared to o_0. On

the end effector, the forward kinematics must be calculated from the encoders measurements for each time step and compare it to the LEDs attached to the tool. In other words, we map the LEDs to fit a calculated point given by the forward kinematics of the robot.

In Geoloc, macros can be created to define frames more rapidly. The macro execute a sequence to define the frames, provided in Step 1 – 7 below. Figure 3.7 is created to support the steps. The figure illustrated the robot, its joints, defined objects, the tool frame and the base frame.

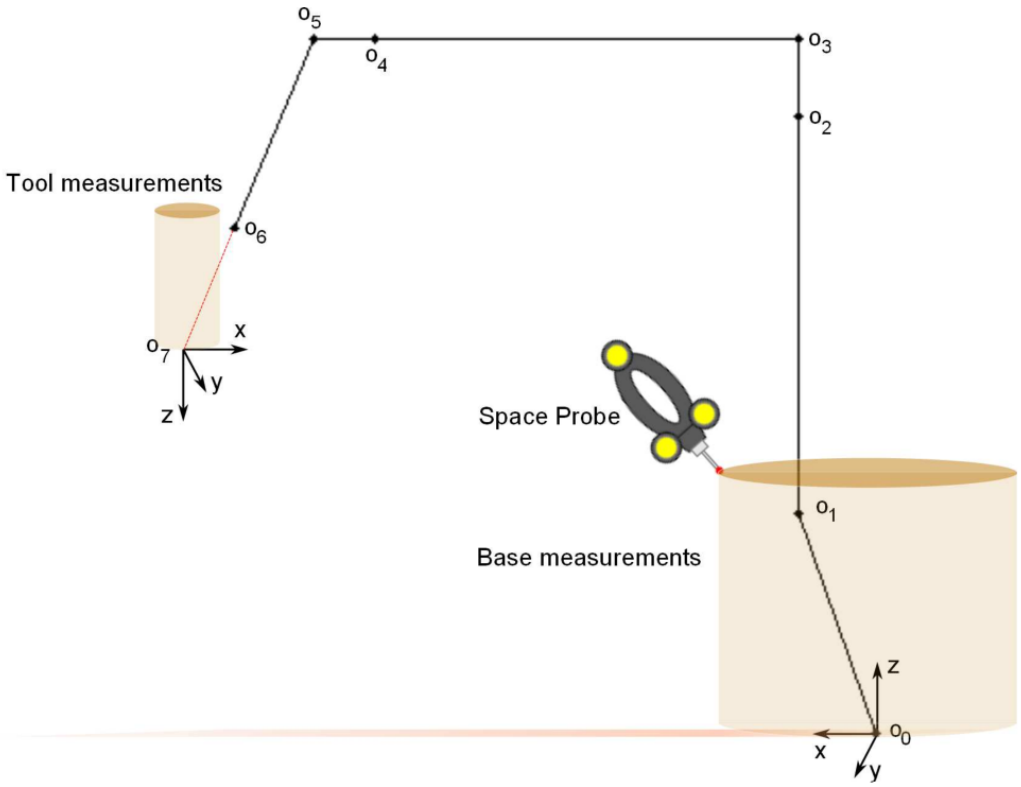

Figure 3.7: Defining Frames by measuring objects around the circumstances of the robot. Cylinders and lines are sufficient to define the frames.

Step 1: Create the base cylinder. The cylinder is created by measuring a plane and a circle on the base of the robot. The plane defines the xy plane where z is zero. Therefore, the plane is defined on the track the robot stands on. The circle defines a normal from the plane which will be the z axis direction.

If the circle is defined by a small rotation in z, there will consist deviations in the final result. Therefore, jogging the robot around its first joint while measuring points around its circular motion will create a clear circle defining the direction of z. The z axis will then intersect through the origin of the robot.

Step 2: Create the base line. As the direction of the x and y is still unknown, a line must be measured to define these axes. In this report, the x axis is defined by finding a line which goes along the same x axis as the robot model. Hence, a coordinate system has been created with the Optical CMM, which approximately is positioned at the same location and orientation as the robot base. It is not required to measure a line to find the y axis since it automatically aligned perpendicular to the xz plane.

Step 3: Create the tool cylinder. The procedure is comparable to Step 1, the difference is that the tool is used to create the cylinder instead of the base.

Step 4: Create the tool line. As Step 2 describes, the x axis of the tool related to the robot model is defined, see figure 3.7. It is arbitrary if the comparison is done with the tool tip o_7 or o_6, since they have the same motions. From o_6 to o_7 it is a simple rotation and translation to align the frame.

Step 5: Create coordinate systems, which related the measurements to the respected LEDs attached to the robot. In this step, it can be compensated for the deviations obtained from the measurements in Step 1–4. Hence, multiple tests must be done in order to compensate for the correct axes. In this step, it is desired to obtain precision which are as close to the robot model coordinate system as possible. Then it is possible to compare the results of the Optical CMM and robot measurements.

Step 6: Create dynamic frames from created coordinate system. Both dynamic and static frames can be created, and they will both record the data that is desired. However, for practical reasons the dynamic frame should be created for both the base and the tool. The tool frame must be dynamic under any circumstances, because the robot will surely move the end effector. The base frame should also be a dynamic frame since the camera can be move around.

Then it is challenging to obtain the same position as before. The problem is solved by defining a dynamic frame. Then the LEDs on the base will always relate the LEDs on the end effector, with the base as reference.

Step 7: Repeat Step 5 and 6 until precision is satisfactory. It is unlikely that the frames will fit the robot at first attempt. Therefore, Step 5 and 6 should be repeated until the frames fit each other.

When the frames are approximately fitted, the following is obtained:

$$o_{7,robot} \approx \text{Dynamic tool}, \tag{3.19}$$

$$o_{0,robot} \approx \text{Dynamic Base}. \tag{3.20}$$

If it is not possible to obtain a satisfactory fit between the frames, new measurements of the objects should be done. Then it is deviation in the measurements, which are inconsistence and it can not be compensated for the them. There exists techniques to obtain accurate fit between the frames from equation 3.19–3.20 in any point in the workspace.

(i) Measure points that are leveled with the axis, which is desired to fit.

(ii) Program the robot to different points in the workspace such that the measurements can be validated.

(iii) The Space Probe must held quietly in one position to ensure quality of measurements.

As both the IRB 4600 modeling and the Optical CMM are described in details, the next step is to develop trajectories, which can be tracked by both systems. The next chapter presents planned paths moving freely in space to observe behaviors, before Chapter 5 examine behaviors when FC is applied.

CHAPTER 4

Chasing Precision of the Camera System

In this chapter, the performance of the IRB 4600 will be studied by creating scenarios developed in Rapid code. The scenarios will provide information and understanding of how the Optical CMM and the IRB 4600 collaborate to commit results regarding position accuracy, motion performance and repeatability of the planned paths.

In order to succeed with such an experiment, it is required to plan both the model setup and the paths precisely. The result will present the performance of the IRB 4600 by comparing measurements from the Optical CMM and the robot encoders calculated by forward kinematics. The work concluded in this chapter will give understanding and experience regarding Optical CMM and the IRB 4600 which will be built further on in chapter 5, Researching Force Control Scenarios.

4.1 Planning

In order to understand how the forces of a machining process affects the IRB 4600, initial experiments must be accomplished to understand how the robot reacts without FC. The path in FC experiments in Chapter 5 is linear based motions with respect to the *Tool Center Point* (TCP). Therefore, it will in this experiment be examined linear motions in free space, which can be useful information for a FC process later.

The linear motions consists of individual movements in x, y and z axis for the end effector. By obtaining measurements from the chosen motions, comparison between the Optical CMM and the IRB 4600 can be performed to find which motions are more efficient.

To conclude which direction is most suited for machining, patterns must be found and it must be discovered if some directions generates more noise. Further investigation will be to examine whether the created path contains the same deviation between the Optical CMM and the robot for a large workspace. Therefore, trajectories at four different spaces will be studied and compared if they include the same behaviors. The procedure of the path generation will be clarified in section 4.1.3, but first, the scenario of the setup will be described.

4.1.1 Calibrating the Camera System

As mentioned in section 3.2, calibrating the Optical CMM is a delicate matter. The sequence of calibration requires time, focus and a steady hand. The goal is to achieve a camera performance with least possible deviation compared to the robot. The procedure of the calibration is described in details in subsection 3.2.4.

To be able to obtain desired precision of the calibration, the sequence of calibration is set to the workspace defined by the edge of the trajectories of this experiment. The workspace area is restricted by the Optical CMM, outside its vision it is not possible to compare data, see figure 3.3 for measurement volume.

The total workspace is user limited by 0.5 m in x direction, 0.8 m in y direction and 0.5 m in z direction, with respect to the robot base. Thus, by calibrating the camera in the edges of the workspace, it is expected to achieve satisfactory precision within the whole workspace. Because of variations in quality of the Space Probe measurements, the results may contain undesired deviations.

The deviations, respectively between the camera and the robot, can vary since it is challenging to measure leveled frames. In order to achieve horizontal frames, the surfaces, which are measured with the Space Probe must be leveled. However, the surface used to define the dynamic base with the camera tends to be uneven and rough, for further explanations see section 3.2.4, Defining Frames.

Several factors tends to be involved to accomplish satisfactory precision, which can be seen in the result of the calibration in section 4.2.1. These result include the comparison of four chosen points at the edge of the workspace, viewed in table 4.1.

The result will give indications of whether the approach method for the calibration also is satisfactory. If the result tend to be unscientific, different approaches will be tested for defining the frames of the Optical CMM.

Path location	**x [mm]**	**y [mm]**	**z [mm]**
a	900	200	650
b	900	1000	650
c	400	1000	450
d	400	1000	950

Table 4.1: Points for quality checking the calibration. These point are located at the edge of the workspace.

4.1.2 Model Setup

For the experimentation in this chapter, two different locations of the camera system will be tested at the laboratory. These locations will consist of different distance and orientation towards the robot station. The reason for examining two different model setups is to examine whether the performance is related to camera placement and LED positioning.

The results of the different camera locations can then be compared to see if the position of the camera affects the performance. The locations of the camera, the workspace and the IRB 4600 are illustrated in figure 4.1. In camera position two it is expected that the workspace is too large, and it will therefore be problems measuring all paths since the camera is located too close. To obtain data for comparison however, it is only required to have measurements from one path from each camera position. From camera position 1, it is expected to receive all relevant data.

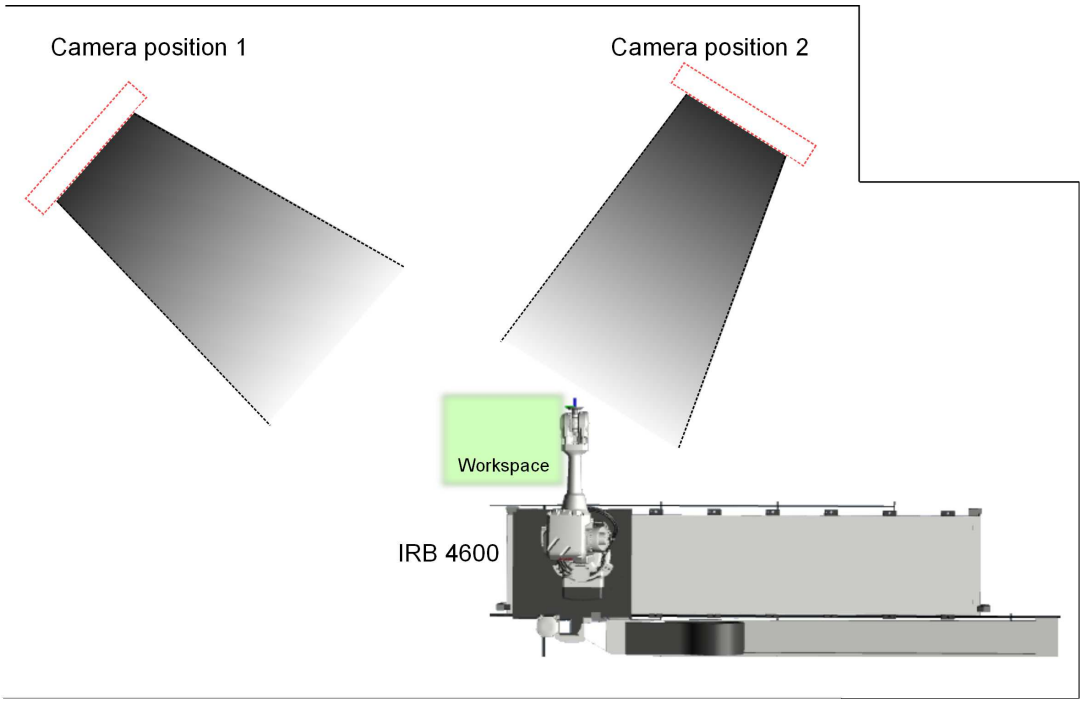

Figure 4.1: Testing two camera positions for the same workspace of the robot. It is desired to find out if the camera positions affects the outcome.

As presented in subsection 4.1.3, there will be four paths in the workspace, where each path has the form of a triangular. If one of the paths in figure 4.3 give data for comparison, with both camera locations, it will give sufficient amount of information about which position is most suitable when FC is applied in Chapter 5, or if the camera location does not affect the performance.

4.1.3 Motion Selection

As mention initially of this chapter the planned path must include linear motions in x, y and z to examine if some directions give is more suited for machining. The same path is copied into four different spaces to examine the behavior for different spaces. Then the measurements can reveal patterns such that future experiments can compensate for the results of the planned motions in this chapter, e.g. direction of the work piece machining.

The path for the experiment consists of a motion through the points p_0, p_1, p_2 and

p_3. The length between these points are fixed for the entire experiment. Then, four different locations of the motion are obtained, referred to as path a, b, c and d for the rest of the thesis. It can then be observed if different locations in the space change the behavior of the robot. The path of the experiment can be seen in figure 4.2, where path a is drawn. For path $a - d$, see figure 4.3. In this figure, table 4.2 is supplemented to view the exact coordinates with respect to o_7.

Path	$\mathbf{p_0}$	$\mathbf{p_1}$	$\mathbf{p_2}$	$\mathbf{p_3}$
a	x = 0.90 y = 0.20 z = 0.90	x = 0.90 y = 0.20 z = 0.65	x = 1.20 y = 0.20 z = 0.65	x = 1.20 y = 0.40 z = 0.65
b	x = 0.90 y = 1.00 z = 0.90	x = 0.90 y = 1.00 z = 0.65	x = 1.20 y = 1.00 z = 0.65	x = 1.20 y = 1.20 z = 0.65
c	x = 0.40 y = 1.00 z = 0.70	x = 0.40 y = 1.00 z = 0.45	x = 0.70 y = 1.00 z = 0.45	x = 0.70 y = 1.20 z = 0.45
d	x = 0.40 y = 1.00 z = 1.20	x = 0.40 y = 1.00 z = 0.95	x = 0.70 y = 1.00 z = 0.95	x = 0.70 y = 1.20 z = 0.95

Table 4.2: Overview of planned paths with respect to the TCP.

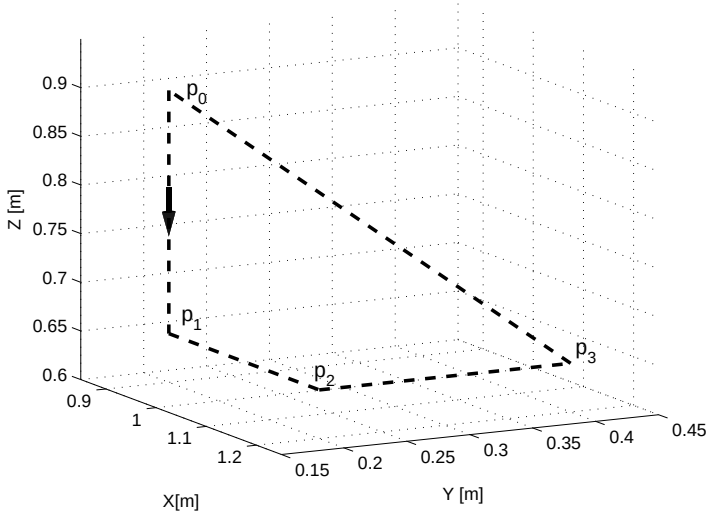

Figure 4.2: Viewing path a for the planned motions.

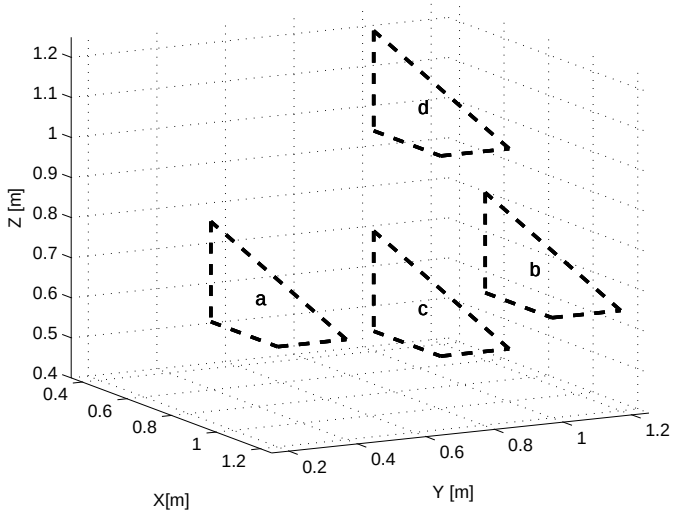

Figure 4.3: Paths a, b, c and d with coordinates in table 4.2. The trajectories are generated by Rapid code.

As one part of the experiment is to study the response in different locations of the room, the limitations of the equipment must be considered. An arbitrary space of the reachability of the robot can therefore not be chosen. The Optical CMM also possess visual limitations, which needs to be satisfied. If a LED appears outside its visual area the measurements will be lost. Thus, the space is chosen to be within the space shown in figure 4.3. This is the same trajectory generated in figure 4.2, reproduced to other reachable and visual areas.

In order to examine repeatability, the robot will execute the same sequence four times for each path in figure 4.3. Each path have the same length in respective directions, whereas $\Delta x = 0.30$ [m], $\Delta y = 0.30$ [m] and $\Delta z = 0.25$ [m]. The velocity for the given sequences is set to 50 mm/s. This is a controlled motion, which is set slow because it is desired to study the deviation between the Optical CMM and the robot, without the presence of centripetal forces generated by high velocity around the joints.

4.2 Results

By executing the planned paths on the laboratory, the result can be inspected by comparing the output signals from the robot with the camera. From the robot it is achieved data from the motor side, which needs to be converted. By including the gear ratio, it is possible to convert the joint angles to correspond to planned motions, see section 3.1.3 for explanations on gear ratio. By deriving equation 3.18, the forward kinematic problem can be solved for each time step in order to find the coordinates of the tool tip with respect to the robot base. Robot coordinates is then compared to the coordinates that are achieved from camera system.

The result is presented in figure 4.4, where an overview of trajectories for a linear velocity of 50 mm/s can be observed. By examining the result further, focus on path a in figure 4.4, which is presented in figure 4.5. It is then more accessible to notice the measurements compared to the programmed path. The deviation between the camera and the robot is presented in section 4.2.2.

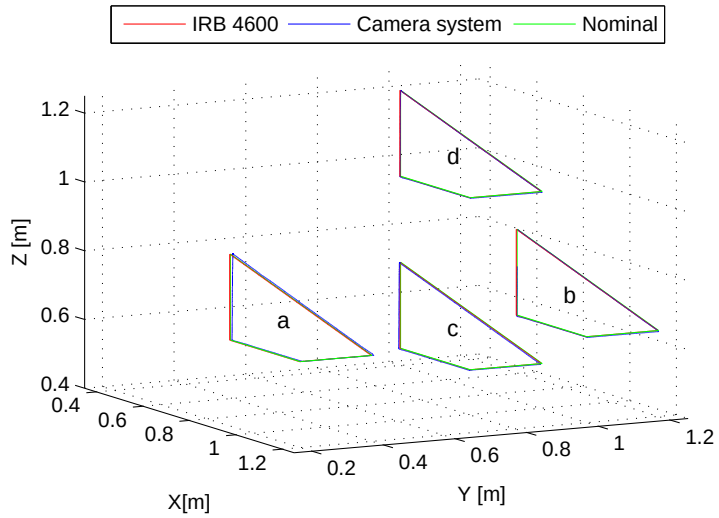

Figure 4.4: Robot and camera system vs. nominal value for planned paths. From long distance view it can be observed that the measurements have similar behaviors.

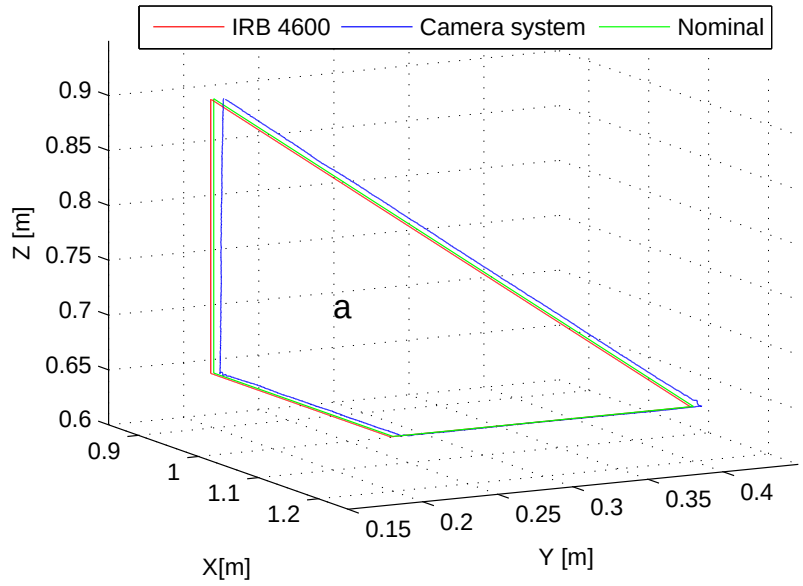

Figure 4.5: Robot and camera system vs. nominal value. By studying the signals closer, the deviations is more accessible.

4.2.1 Camera Calibration

In this section, the result of the adaption of the Optical CMM will be presented. For each point in figure 4.1, there are quality assurance by repeating measurements three times. Since it is known from derivations of the forward kinematics, the exact point given by the robot, the Optical CMM can be adjusted to map the frames to fit the robot frames, as explained in section 3.2.4.

As the robot is programmed to the four different coordinates in table 4.1, the robot can move back and forth until a satisfactory calibration is obtained. Hence, quality assurance of both repeatability and robustness globally over the workspace are obtained. In the presented results, it is focused on the deviation between the camera coordinates and the deriving of the forward kinematics of the robot. Since two different camera locations are tested, the quality assurance must be completed twice because the LED placement between the experiments is changed.

Figure 4.6 shows the result the deviation of each path for camera position 1, and 4.7 shows camera position 2. It is focused on illustrating the deviation from the

point in space calculating by the forward kinematics as explained initially. The measurements are originally 3D points in space, which give complications when it is desired to examine the least possible deviation for each axis. Therefore, the measurements are split into three subplots illustrating the deviation for the xz, xy and the yz plane. Hence, more tuning of the dynamic base or tool in the camera system will give improved deviation in some points. However, it will worsen deviation in others since there exists measured points spread around the reference point.

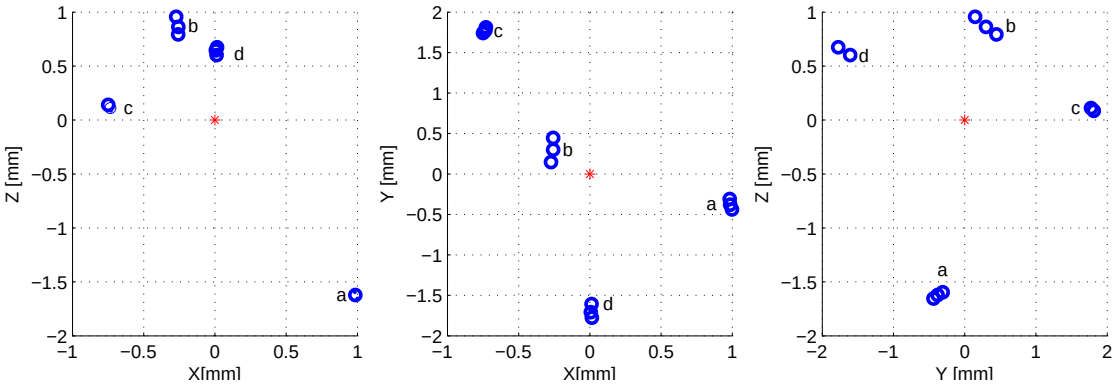

Figure 4.6: Deviation of the camera calibration for camera position 1. The calibration points are spread around the reference.

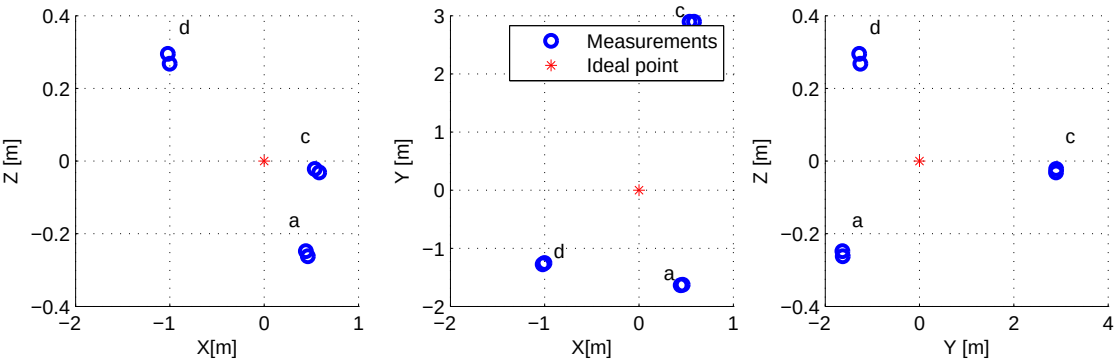

Figure 4.7: Deviation of the camera calibration for camera position 2. Similarly with figure 4.6, the measurements are randomly spread around the reference, caused by the Space Probe measurements.

The issue of not finding reference deviation can also be verified in figure 4.8 and 4.9. In these figures, the stochastic behavior of the points in different coordinates is present. The ideal line in these figures are at zero, ideal here means the reference given in table 4.1. Optimally the points should be one straight line at zero. The second camera position miss the result of path *b*. The reason is that the line of sight is outside the limitations of the camera. More of the reason for the behavior will be considered in the Discussion in section 4.3.

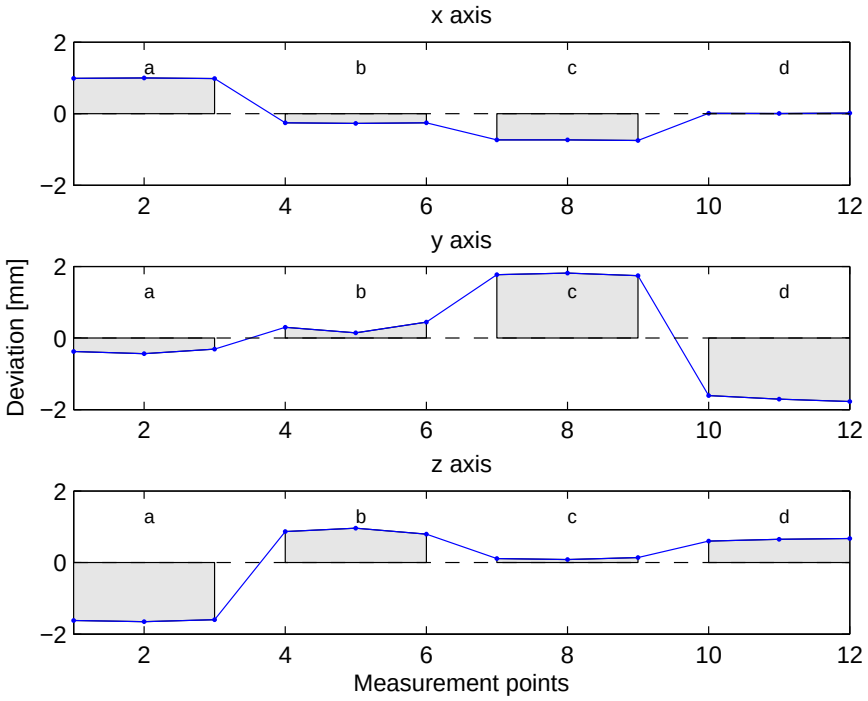

Figure 4.8: Deviation for camera position 1, calibration in x, y and z axis. Each calibration point a–d are measured three times.

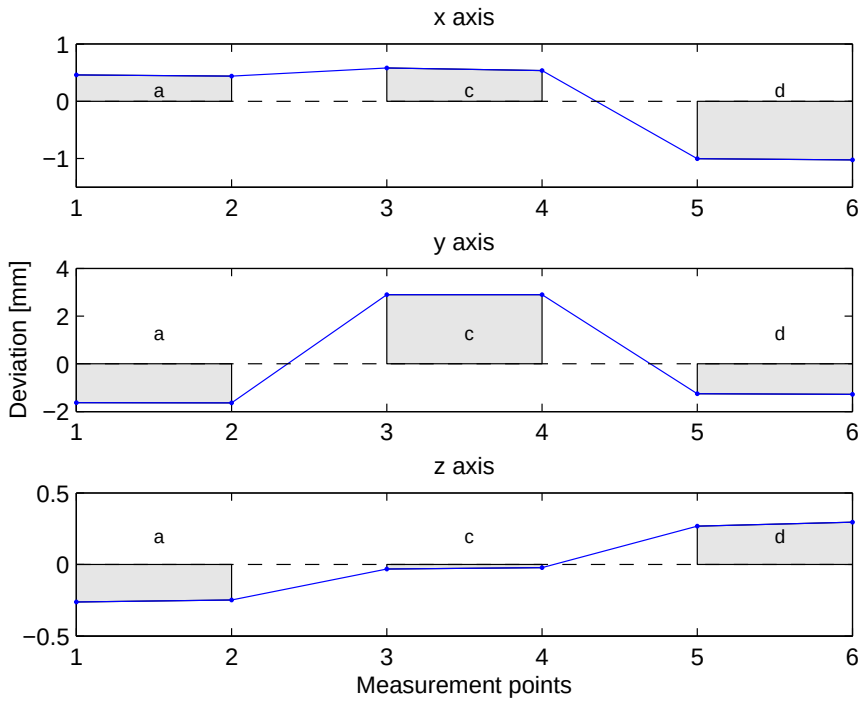

Figure 4.9: Deviation for camera position 2, calibration in x, y and z axis. The measurements are different from position 1.

4.2.2 Deviation Between Camera and Robot

As it is desired to examine the behavior of both the camera system and the robot, it is required to find the deviation from the planned paths. From the 3D perspective (figure 4.4-4.5), it is difficult to study the deviation. Thus, the deviation is studied by examining each individual signal from figure 4.4. Since the robot and the camera have different sampling time, the signal with highest frequency must match the other to be able to compute deviation without loss of dynamics. Since the robot encoders sample every 4.032 ms, the signal must be converted to fit the camera of 10 ms sampling period.

When both the camera and robot measurements have the same sampling period it is still required to know when the measurements begin with respect to each other, this issue is discussed in section 4.3. Since the camera and the robot operates on two different softwares and computers, time shift optimization would be impossible

without a connection the computers.

There exists no connection between the computers in this experiment, the comparison between the camera and robot will be a theoretical fit between the signals. Thus, by utilizing cross correlation from section 2.2.4, time shift of one signal is performed to match the other as the least deviation between the two signals is calculated.

When start and stop time is synchronized, the signals can be compared. The signals desired to study are the raw data from the robot, computed by forward kinematics of the joints, and the camera system measurements. By computing the deviation of these signals from the robot reference signal, the deviation as a function of time can be plotted. Since four different paths are measured, a large amount of data are obtained.

First, figure 4.10 is presented, which plot x, y and z as a function of time. The comparison is done between the robot raw position versus the camera, robot reference versus the camera, and the raw position versus its own reference. From time $0 \rightarrow 5$ the trajectory move along z, time $5 \rightarrow 10$ along x, time $10 \rightarrow 15$ along y and $15 \rightarrow 25$ along xyz.

It can be observed that some direction provide less drift off than others do, i.e. the x direction between 5 and 10 seconds tend to be more satisfying than other directions. The z measurements is also horizontal at this measurements, but has a large offset of 1.5 mm. The noise of the camera tend to be different for the different axes, especially for the y measurements.

To observe if the tendency of the deviation between the Optical CMM and the robot encoders data is similar for every path planned, observe figure 4.11. The figure shows that the same pattern is measured, but it can be observed different offset for the axes. There also occur oscillations for path c in the y axis, which is nonexistent in the other paths.

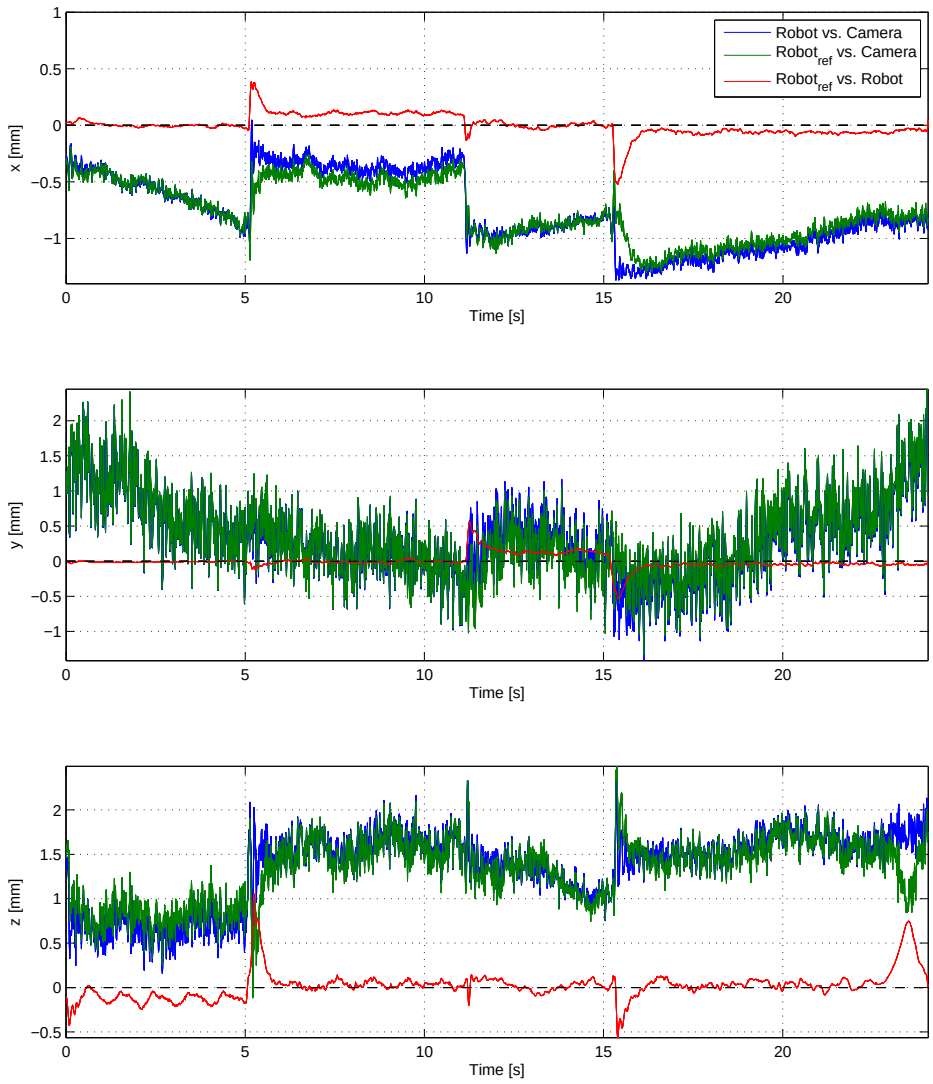

Figure 4.10: Robot and camera system trajectory for path a. The deviations reach up to 2 mm, but by picking out a minor series it can be achieved smaller deviations, i.e. from $5 \rightarrow 10$ seconds for x.

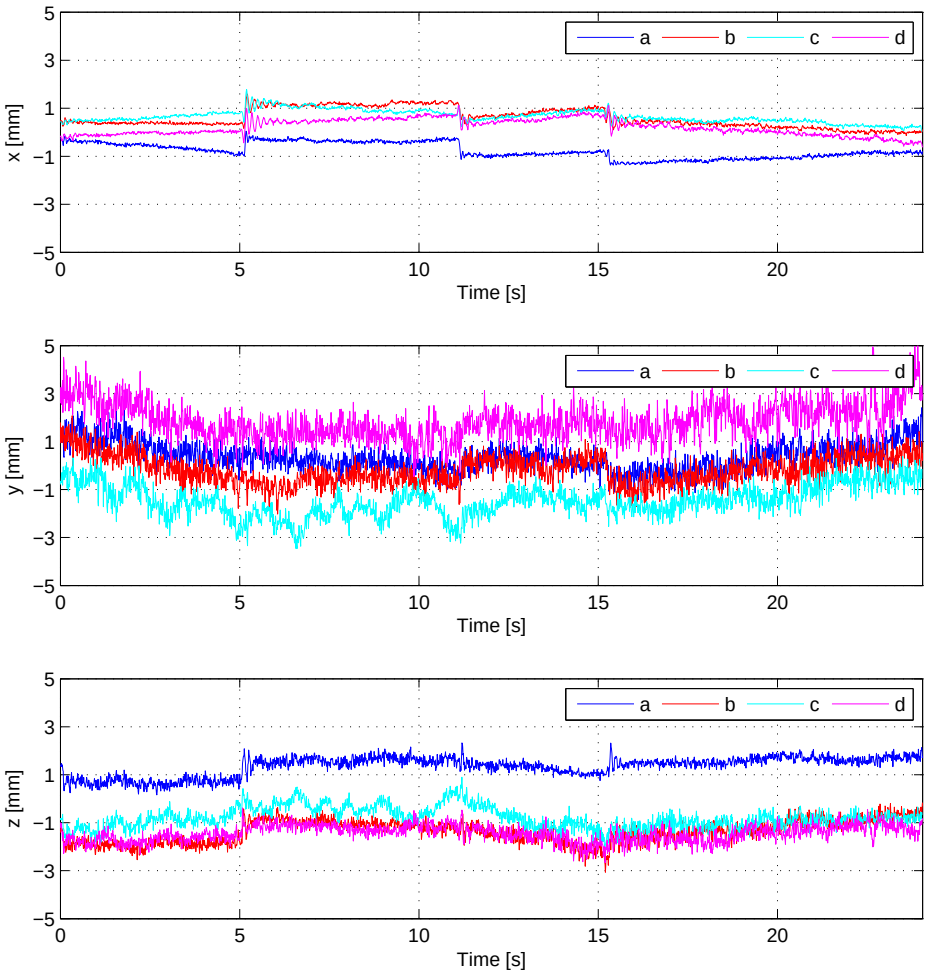

Figure 4.11: Deviation for path a to d. The different paths have similarities, but the performance vary for different robot configurations.

4.2.3 Repeatability

In order to observe whether the paths are repeatable, the sequence is repeated four times for each path. There is however, only three sequent measurements available for path b, because the last run possess an unscientific outcome. The repetitiveness is plotted in figure 4.12, where x, y and z is plotted for the different paths in four subplots. Since the measurements in figure 4.12 are noisy it is in particular difficult to view each individual signal.

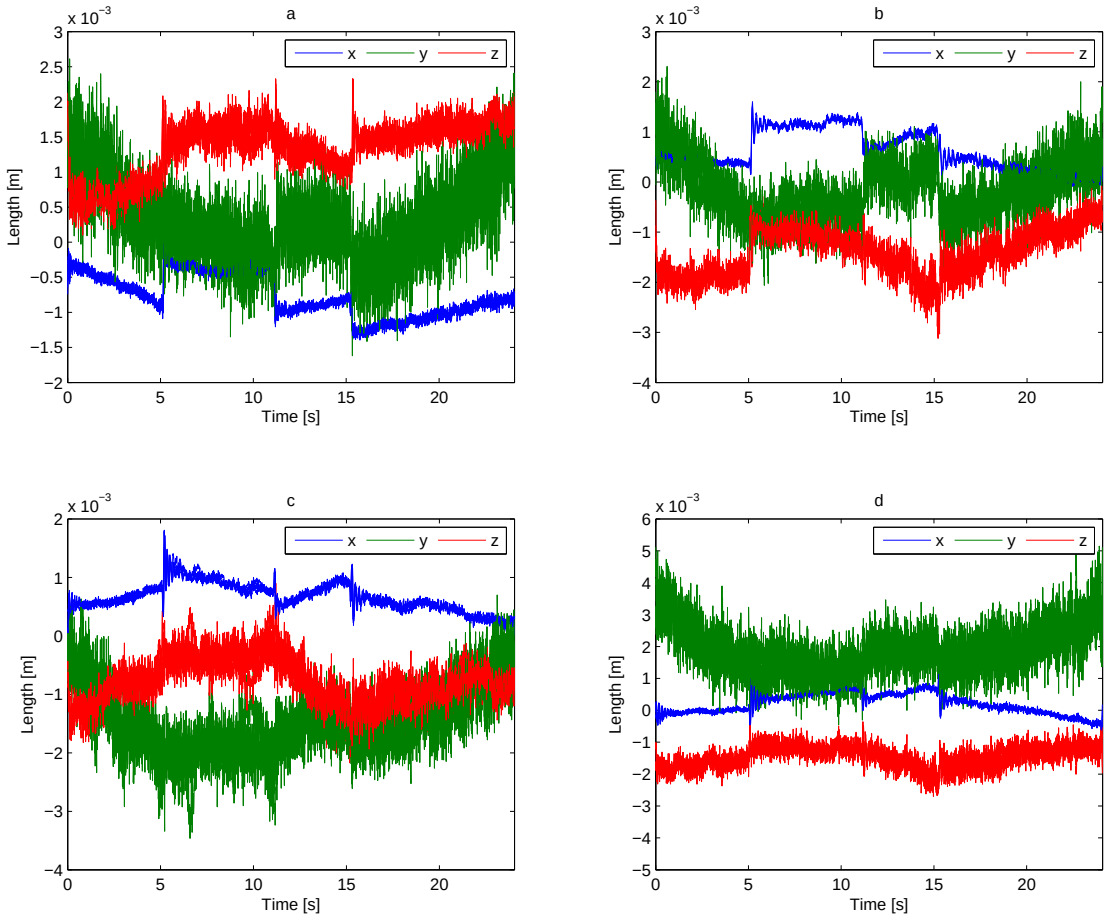

Figure 4.12: Analyzing repeatability for each path. Each path is repeated four times in camera position 1, where the deviations in x, y and z is presented.

The signals can be detected on top of each other in figure 4.12. The numerical outcome must also be derived to confirm that the signals are repeatable. By computing the least absolute deviation, the $\mathcal{L}_1$ norm, for each sequence, the deviation for each signal can be viewed, numerically. The computation give an indication of the repetitiveness for the deviation, presented in table 4.3. The $\mathcal{L}_1$ norm is defined in *Robust Adaptive Control* by A.Ioannou and Sun [5] as $||x||_1 = \int_0^\infty |x(\tau)|d\tau$.

Sequence nr.	**a**	**b**	**c**	**d**
1	6.35	5.99	7.08	8.76
2	6.24	6.04	7.10	8.78
3	6.17	6.20	7.01	9.01
4	6.26	–	7.04	8.86

Table 4.3: $\mathcal{L}_1$ norm of the deviation between camera and robot measurements. The values do not change much between each run and the deviation is stochastic around a set-point

4.2.4 Comparing Camera Positions

In this section, the location and orientation of the camera system are changed as shown in figure 4.1 to position 2. To compare, it is sufficient to analyze one path. Thus, the result compare path a, where the computed deviation is calculated between the camera and the robot. It is expected to achieve curves, which follows each other within small deviations. The result is presented in figure 4.13. It can be observed that the deviations are within 2 mm most of the trajectory, between the two camera positions. However, between 12 and 15 seconds the deviations between the positions in z raise up to 3 mm.

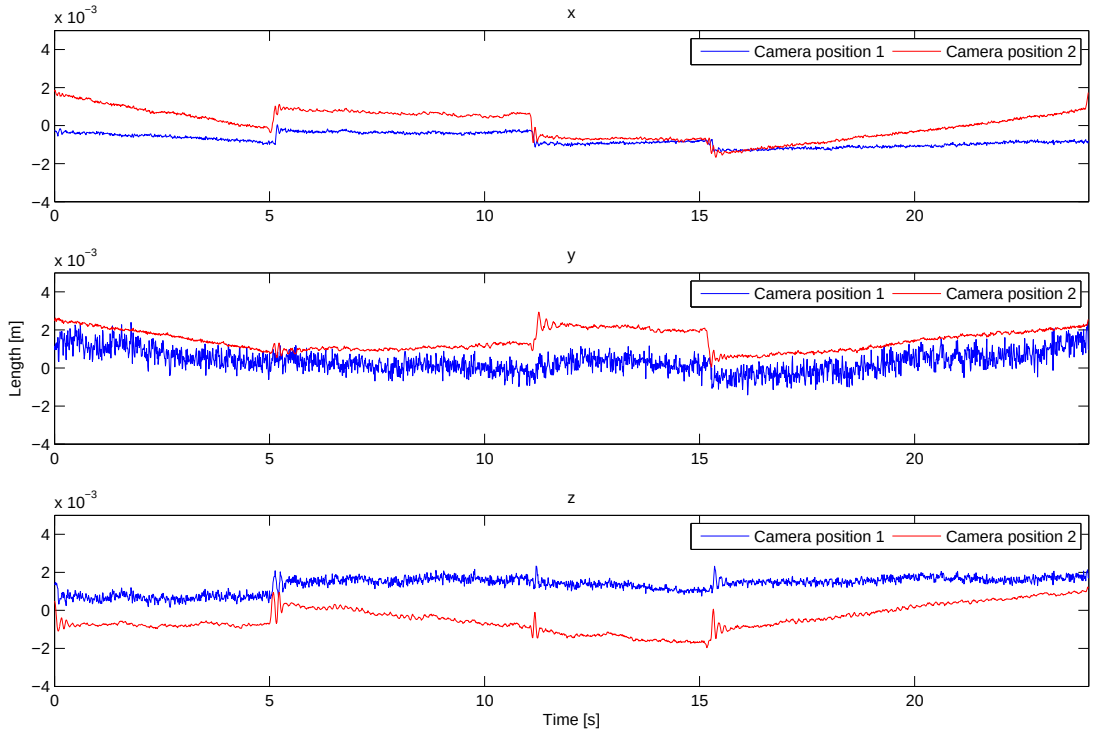

Figure 4.13: Comparing measurements from camera position 1 and 2. The deviation are similar under certain workspaces, but is shifted elsewhere.

4.3 Discussion

Experiments done in this chapter possess results which occurs intermittent by reason of the setup scenarios described in section 4.1.2. The complication for any experiment utilizing the camera system is that the camera must stand in one position while calibrating. If it is changed, new calibration must be done from scratch, because the Space Probe measure frames on physical objects. A major part of the deviations, are reasoned by measurements done by the Space Probe. It is also very time consuming to accomplish precision with the camera system that give satisfactory results.

Inaccuracy Caused by Defined Frames

The reason why the camera must stand in one position while calibrating with the Space Probe, is because that the LEDs attached to the robot relates frames to given coordinates. The LEDs provide information of where the end effector is located with respect to the dynamic base frame. The problem is, when calibrating the robot in one position, the deviation between the camera and the robot will increase the further away from the reference point the end effector is located.

The deviation occurs because the orientation of the dynamic frame is slightly rotated around each axis. Thus, a deviation will increase longer away from this point since the deviation between the dynamic tool frame and base frame increases. This is the reason for why calibrating the camera system is time consuming. As a improvement, the camera system was quality checked in four different programmed points for the robot. In this way, there exists four references to adjust the camera frames towards.

By moving the robot while calibrating, the potential of errors increases because the robot might not go back to the exact position for each calibration cycle. For a point, ABB Group states that the robot can repeat a position within 0.05-0.06 mm, see Appendices *IRB 4600 Industrial robot*. When having deviations up to 1-2 mm, the main error is not in the robot, but in the camera calibration. Because of the deviation in each repetition of the robot, the camera frames might be adjusted in the wrong direction for each run.

Positively, by checking the calibration in different points, the probability of deviation between the camera system and the robot over a larger area is decreased. The procedure require more time, since the robot must go through four different points multiple times. After performing multiple adjustments and finding the mean of the deviation, the smallest deviation for the measurements, performed with the Space Probe is found.

To accomplish ideal measurements, the objects measuring on, must be leveled with the robot such that the frames are aligned and rotated perfectly. Because of measurement noise existing in the signals, ideal frame definition is not possible.

There will however be, achieved measurements close to theoretical values. Solutions which can generate minor deviations exists, which will be detected in section 5.2.1.

The reason for conducting the experiment was to observe the performance of the IRB 4600 in straight lines. Especially in the x and y direction, which is most similar to a finishing process. Until now, measurements are observed as a function of time, but the measurements can also be studied as a function of the length traveled in the path. As the motion along x and y is most relevant, the study will focus on how the deviation in z_{dev} behave as function of these lengths, in other words

$$x(t) \implies x(z_{dev}), \tag{4.1}$$

$$y(t) \implies y(z_{dev}). \tag{4.2}$$

The new way of observing the behavior can be seen in figure 4.14, where the measurements along x and y with the deviation z can be viewed.

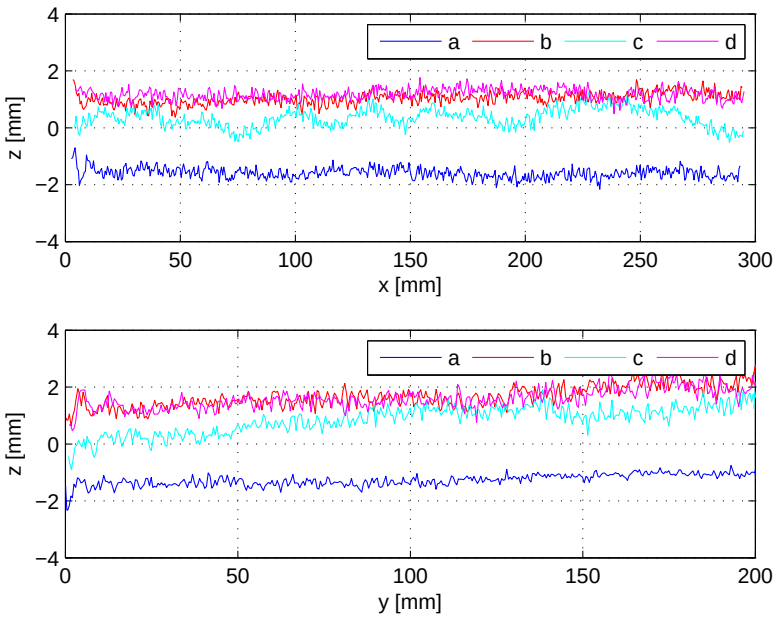

Figure 4.14: Deviation between robot and camera as functions of $x(z_{dev})$ and $y(z_{dev})$. In the minor workspace depicted, the deviation only contains an offset.

There are three elements which can be summed up by observing figure 4.14 and experiences done previously in this chapter.

(i) An offset is experienced at each path a, b, c and d. The offset comes as a reason, which is mentioned initially of the discussion that there exists a rotation in the dynamic base defined by the camera system. Thus, the deviation will increase for paths, which are further away optimal calibrated point. The observation can especially be seen in figure 4.13 for the y axis. The measurements have minor deviations at 10 to 15 seconds, but drift off between 0–10 and 15–25 seconds.

(ii) By noticing figure 4.11, it is noticed that measurements have an unexplainable drift. The drift seem to be inconsistent, causing issues for the analyzing. The drift can however, be limited if the focus is a minor workspace. From figure 4.14 it can be seen when plotting $x(z_{dev})$ and $y(z)_{dev}$, that it can be achieved straight lines which are almost leveled with the robot if the calibration is properly done. The experiences of improving calibration will be brought into the next experiment, when comparisons will be done when FC is applied.

(iii) Even though the paths have identical path movement and velocity, the signals tend to have different characteristics, see figure 4.14. Then, especially in the x axis where path c tend to have periodic oscillations. By recalling planned paths in table 4.2 and the corresponding figure 4.3, it can be seen that the reason might be the position in space for path c. The robot lean more to one side, which may cause the low frequency oscillations. It might also be the position of path c corresponding to the camera position. One possible solution can be that the path is located at the edge of the measurement volume of the camera system, such that the LEDs is challenging to detect.

Sampling Time Strategies

The robot utilize encoders to track data from its position, which has a sampling time of 4.032 ms, on one software. The Optical CMM operates on a sampling time of 10 ms on a different software with no connection with the robot. This

complicate the procedure of finding the deviation between the signals such that they match each other.

The procedure, which use cross correlation, is only a theoretical approximation. Since the signals operates on two different softwares on two different computers with no connection, it is impossible to predict the actual time the signals are shifted with respect to each other. Thus, by time shifting using cross correlation, it is assumed that the time can be fitted to the start and stop for the robot motions.

In reality, perfectly matched motions may not be the solution because of delays in the gears of the robot. If connection between the softwares existed, it would be expected that the camera is delayed from the robot. The delay is caused by that the robot send signals before we have a physical reaction, which the camera system are able to measure. The delay is illustrated in figure 4.15, where lag is an unknown constant. Without connection, cross correlation is a satisfying tool to compare the camera and the robot since the start and end of movement is known.

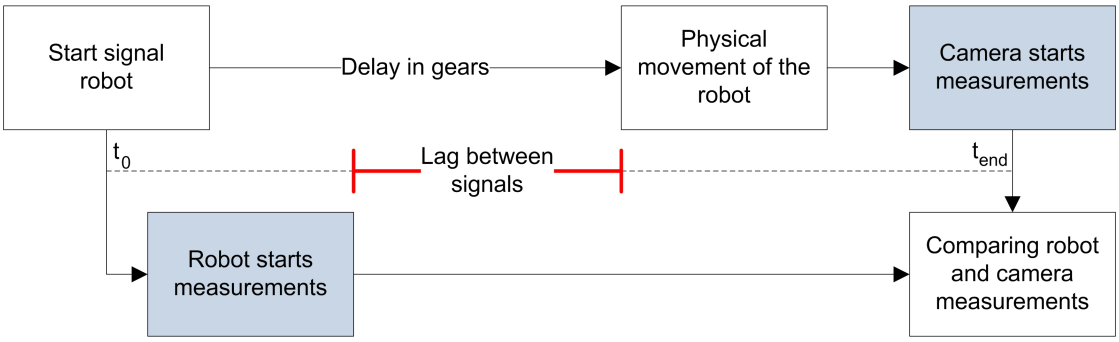

Figure 4.15: Flow diagram of signal measurements. The camera measurements are delayed with the respect of the robot because of minor slack in gears.

Noise Related to LED Placement

By looking back at the two different camera position measurements in figure 4.13, it can be noticed that the same measured signal has different noise for two individual camera positions. The same signal here means the same path, which is path a. At first, the behavior seems strange, since the robot moves the same path at both cases. Regardless of the same motion, the measurements from the camera tend

to be different. A reasonable explanation can be that the changed LED location produce different behaviors because of depth and width of their placement. It cannot be taken any sure conclusion for the misbehavior, but there exist facts that may cause it. In camera position two, the camera is located closer to the robot. A closer position may produce a smoother signal.

The area, which are accessible for measurements however, decreases when closing up on the robot. This is a problem when it is required to measure larger areas with the camera system. Another element that may cause noise is the actual placement of the LEDs. If the LEDs are spread out more with different depths, the achievement is a more robust signal. If the LEDs are placed within small margins, the camera can have difficulties reading the data correctly. Thus, it affect the frames created from the physical objects. Therefore, the LED placement on the tool seems flawless for camera position two, only disturbed by minor noise components. For camera position one, the depth in y is most likely too weak, and should been placed with more depth. This means the LEDs was placed approximately planar with respect to the xz plane for camera position one.

Since there exists unanswered questions regarding the frequency components of the different paths from figure 4.14, a wider research must be done. It is desired to study if the frequency components match and to observe which frequencies are dominant.

The frequencies can be analyzed as a function of energy, and by using the theory from section 2.2.3, the PDS can be plotted. The PDS can be seen in figure 4.16 where the frequencies of $x(z_{dev})$ in figure 4.14 is plotted. Figure 4.16 declare that every path attain the same frequency components, with different power. The low frequency components of path c is difficult to notice, since it seem to be part of the direct current (DC) component in the PDS.

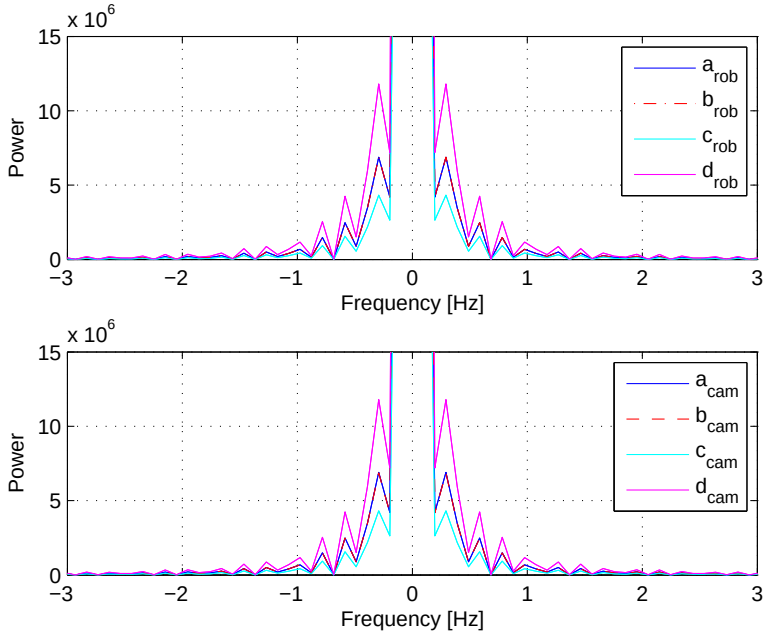

Figure 4.16: PDS of the path a, b, c and d. The top figure is x measurements and the lower represents y for the robot.

This chapter has given understanding and experience of both the camera system and the industrial robot. It was seen that the procedure of defining the frames was not optimal, and it will therefore be compared to a new method when FC is applied in Chapter 5. Instead of performing paths when moving freely with the robot, the next chapter will focus on trajectories when contact with an object is applied.

CHAPTER 5

Researching Force Control Scenarios

This chapter investigate behaviors of the IRB 4600 when FC is activated. The scenario will be developed by including FC experiments with different forces. The focus will be to examine performances while in contact with an object without grinding. Therefore, a tool with a wheel will be developed to make such a scenario feasible. The outcome will have similarities of a machining process. The main difference is the direction of forces applied to the process. Analysis of the motions will still be compared by the camera and robot data.

To this experiment the focus will be to apply FC in the z direction directly towards a metal plate while moving along it. The goal of the experiment is, by studying the motions of the IRB 4600, to find characteristics in the robot behavior, which should be compensated for in a machining process. The outcome of a machining process tend to be rough, therefore the performance will be studied such that future experiments can develop compensating controllers. In this way, the final product of a machining process can be improved. To view the planning of this experiment, see section 5.1. The results of the developed experiment can be seen in section 5.2. For supplementing materials on FC review the ABB products *Application manual* [1], *Function Package IRB 4600* [3] and *Test Signal Viewer* [4].

5.1 Planning

The planning of the experiment will be to develop a scenario such that the goals, which was established can be completed. Therefore, a tool that has the form of a rod with a wheel attached must be designed, replacing the drilling spindle. Afterwards, execution of experiments including contact along a chosen object with

different pressure forces is applied. The measurements will consist of the camera position, robot position and FC signals from a program called *Test Signal Viewer* (TSV). All three softwares operates with different sampling time, such that a down sampling for both the robot encoders of approximately 250 Hz and the TSV of approximately 2000 Hz, must be performed to fit the sampling time for the camera of 100 Hz. The path for the FC scenario will be developed to have contact along a horizontal metal plate. The wheel at the end of the robot will face the linear direction of the motion such that friction forces are minimized. Friction is therefore not monitored in this experiment. For an example code of the FC in Rapid code, review the Appendices for *Example Code of Force Control*.

5.1.1 Tool Design

In order to perform experiments with FC, a tool must be designed which can go along a surface and keep constant pressure along the path. Therefore, the tool require a wheel at the tip such that friction forces are reduced. The wheel is designed to go along one direction without the ability to rotate. Movement in a straight line is most relevant because it is more similar to a grinding process. Therefore, it is not necessary to do a rotational move for this experiment. The construction of the tool must be rigid, in the way that it will not be damaged when the robot applies a force to the object. The length is chosen to be approximately 200 mm, and the diameter is 16 mm. The tool design can be seen in figure 5.1a, and the attachment to the robot in figure 5.1b. The tool in figure 5.1a is designed in the software SolidWorks consisting of three components. These components are the rod, a wheel and bolt which connects the wheel and the rod.

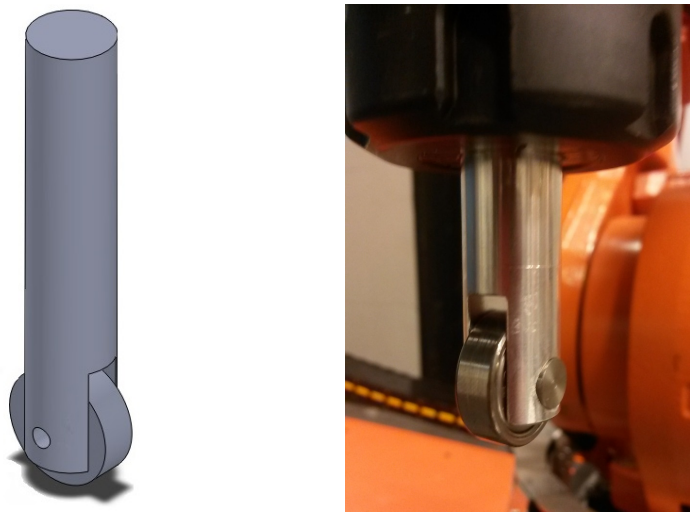

(a) Tool design. (b) Tool attached to robot.

Figure 5.1: Tool design from SolidWorks and the product attached to the robot.

5.1.2 Calibrating the Camera System

The camera is chosen to be located in camera position 1, as witnessed in the previous experiment (figure 4.1). This position has larger workspace and the camera is more operational and flexible. Since a new camera position and a new LED placement is used, the camera must be calibrated again. The workspace is chosen to be limited at the process area of the experiment. Thus, the camera will be calibrated from the approach point to the withdraw point of the FC operation.

As experienced in Chapter 4, the camera measurements and calculations for robot encoders do not have similar motions. The camera measurements tends to drift off and have different offsets when comparing to the robot. It has been assumed in the Discussion of 4.3 that the dynamic base of the camera corresponding to its LEDs is not properly defined. Therefore, an other method must also be considered.

The idea include a new definition of the dynamic base when measuring with the Space Probe. Step 1 in subsection 3.2.4 for frame definition is therefore changed. Instead of creating a cylinder object, which defines the base, a circle and a plane are defined instead. The circle is defined as before, by measuring when jogging the robot around its first joint. The new aspect is the plane definition, which now is

measured on the work piece itself, i.e. the metal object.

The goal is to have a dynamic base frame in the origin of the robot which is leveled with respect to the work piece which is applied force, and possibly leveled to the robot base o_0. The new frame definition can be viewed in figure 5.2. By proceeding with measuring on the work piece, it is expected that the comparison with the robot and the camera measurements will be leveled with respect to each other.

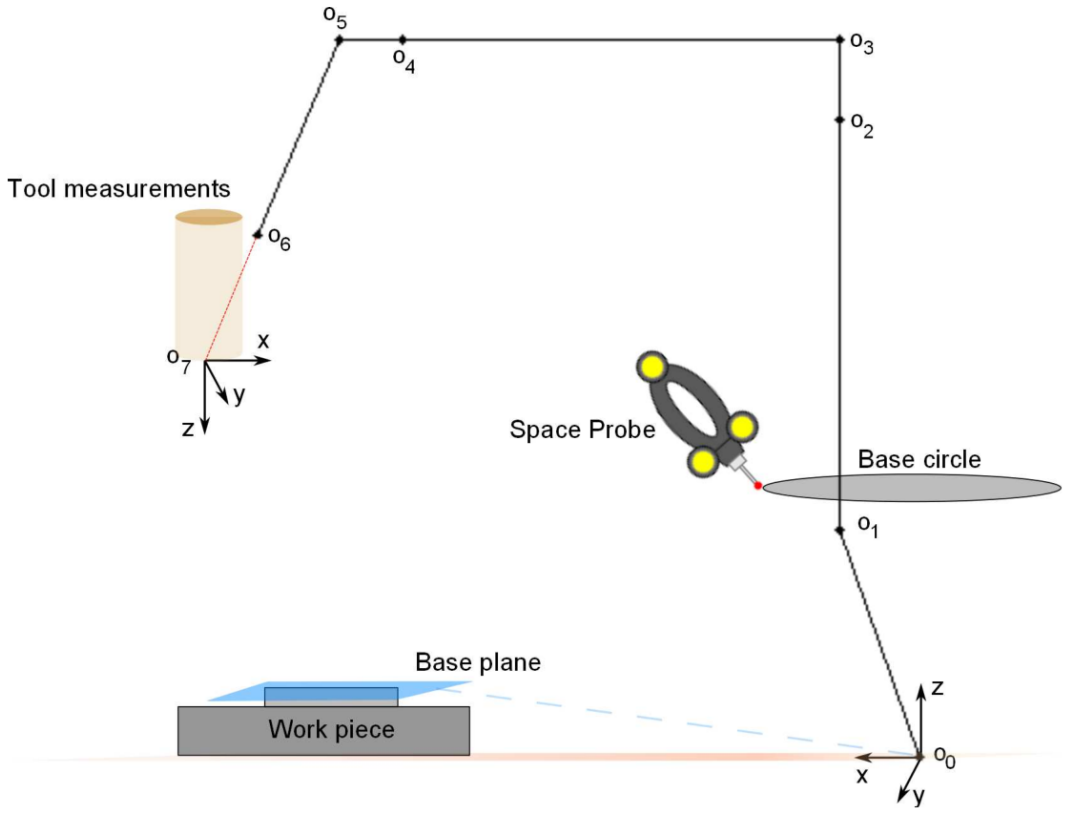

Figure 5.2: Defining dynamic base by measuring on work piece. The work piece is leveled with a tool and the measurements are shifted towards o_0

The level with respect to the robot base however, is not guaranteed. This level is influenced of how leveled the work piece actually is placed. It is assumed, that the comparison between the robot and the camera will behave more similar at the work piece. This assumption is made by the fact that the work piece has a flat

surface, which can be seen in figure 5.3. When measuring the new plane, a shift must be applied in the z axis of 280 mm in order to have the same height as the robot base. The results of the camera calibration will be given in section 5.2.

5.1.3 Trajectory Selection

The trajectory for this experiment is chosen to be of same character as a machining process. Therefore, a path is developed which can keep constant pressure against the object in figure 5.3. The tool with a wheel is sufficient to create such a trajectory. The wheel of the tool must always point in the direction of motion, or else the robot will experience undesired friction forces. For the experiment, only one path is necessary, and can be designed by teaching the robot while moving it to specific locations in the workspace. The path will be repeated multiple times with forces applied to it between 1 and 50 Newton. The main procedure of the trajectory is given by three stages, which is:

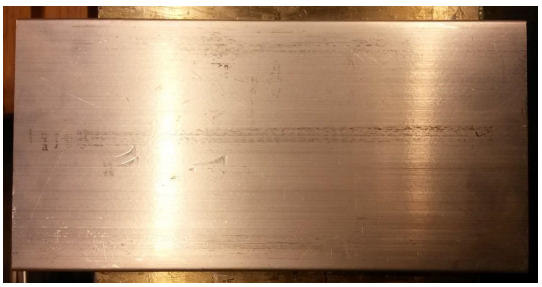

Figure 5.3: Metal Bar, 20×10 cm.

$$\text{Approach} \rightarrow \text{Process} \rightarrow \text{Withdraw}.$$

The steps above are applied to the path while at the same time recording with the camera system. The path is illustrated in figure 5.4 where the approach point is at $x = 0.9485$ m and the withdraw point is at $x = 1.0862$ m. It can be observed from the figure that the force is only applied to the object under the pressure process. It is aimed to have five runs with different forces against the object to reveal patterns with the camera system. The forces are applied in the negative z axis, which is the same direction as the gravity forces.

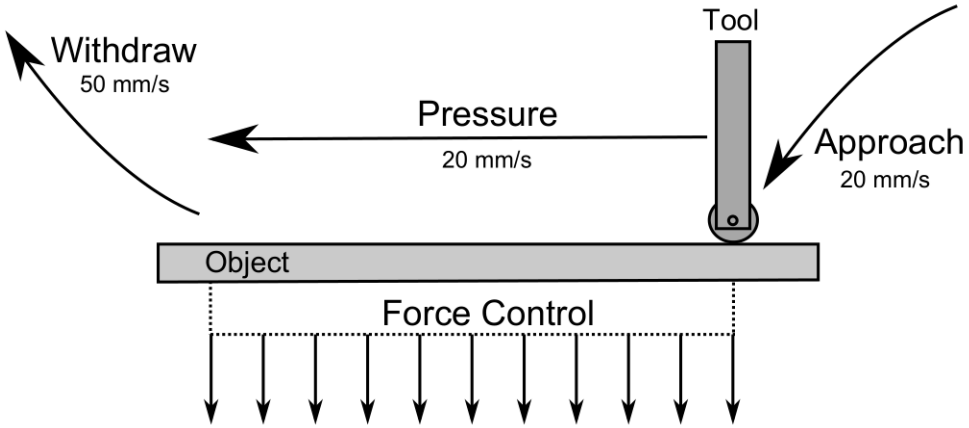

Figure 5.4: Planned trajectory where the robot approach with 20 mm/s and continue with the same velocity until the withdraw point.

All the runs with different forces will follow the same programmed path as seen in figure 5.5. In this figure it can be seen that Z_{p+} defines the positive z axis. Thus, force is applied in the Z_{p-} direction, which is directly at the object. Figure 5.6 give a perspective of the same path, where the robot is drawn by deriving the inverse kinematics, see section 3.1.2 for calculations.

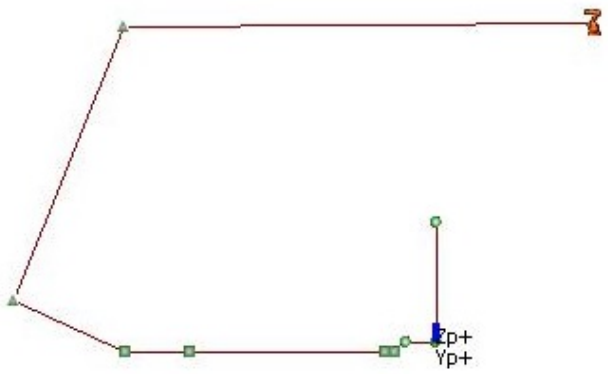

Figure 5.5: Path created by *Human Machine Interface* (HMI) on-line programming.

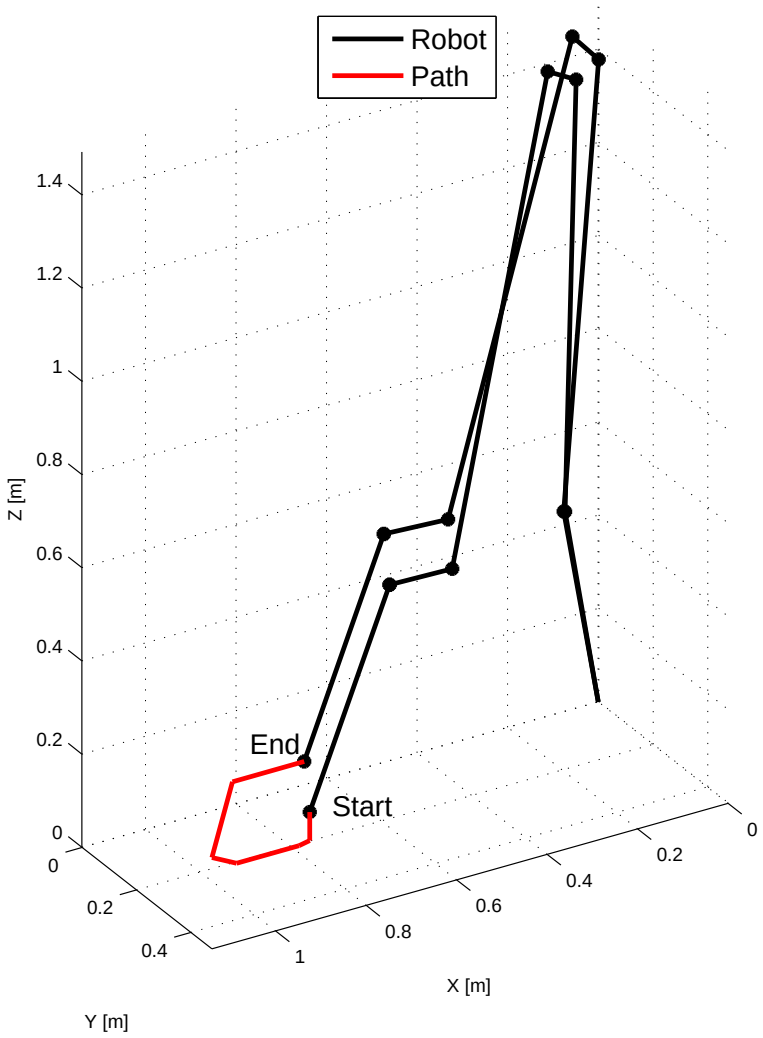

Figure 5.6: Path shown from MATLAB.

The approach of the trajectory aims to touch the object approximately 1 cm within the edge of the metal bar. It is then assured that the wheel is always in contact at the flat. The approach point can be seen in figure 5.7b. The robot also aim to withdraw approximately 1 cm away from the edge as seen in figure 5.7a. The procedure of the planned forces in the experiment can be seen in table 5.1, and the outcome is presented in the Results 5.2. It can noticed that for the work piece

calibration, an additional force of 5 Newton is added to study the behavior at minor forces.

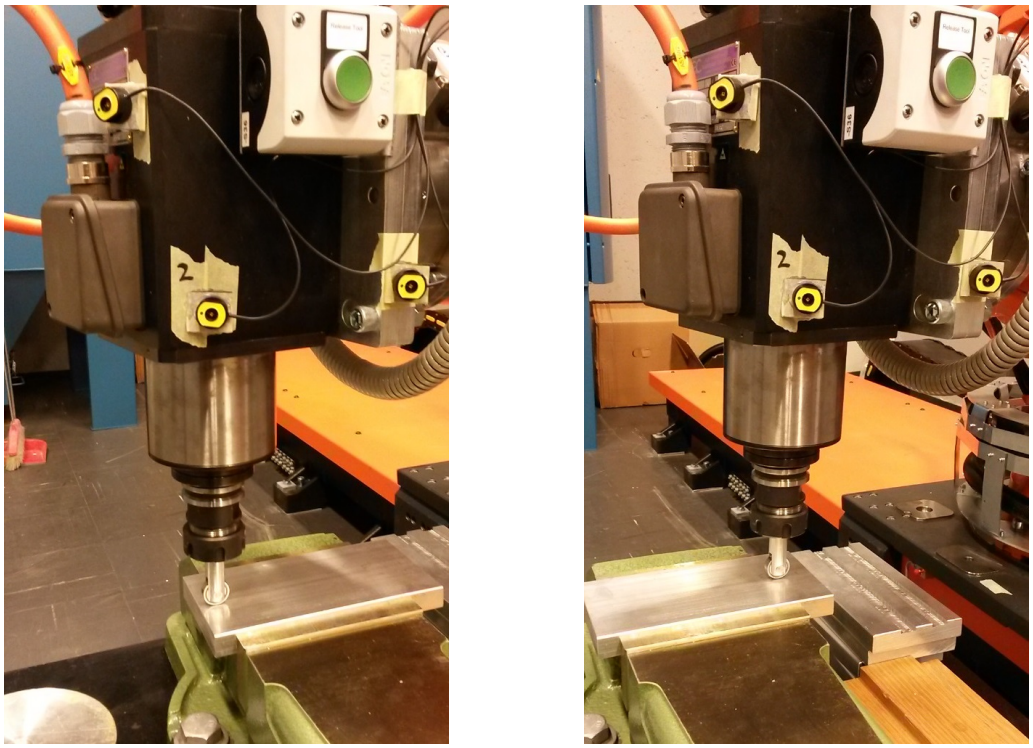

(a) Withdraw point.

(b) Approach point.

Figure 5.7: Robot position at process start and end. The camera system is also calibrated at these two points for the robot tool.

Run nr.	1	2	3	4	5
Force applied [N] in base experiment	1	10	25	50	-
Force applied [N] in work piece experiment	1	5	10	25	50

Table 5.1: Forces applied in the experiment. The result will present the outcome for both calibration methods.

5.2 Results

For the results, three different aspects will be studied. The first aspect is the Camera Calibration (5.2.1) where it will seen results of the camera calibration for both the methods in section 5.1.2. Then, a study of the outcome for the forces in section 5.2.2 will be presented. It is desired to examine if the planned forces against the object exists as intended. At last, a research of the the deviation between the camera and the robot will be presented in section 5.2.4. This section will reveal whether the robot and the camera measurements are equally for the different forces applied.

5.2.1 Camera Calibration

As mention initially in section 5.1.2, it is required to calibrate the camera repeatedly because of a new location from the LEDs for the experiment in Chapter 4. As experienced from the test in Chapter 4, changing between camera position 1 and 2 (figure 4.1) are not the reason for the deviation which was observed. Because of unwanted behaviors, an alternative method was planned for calibrating of the Optical CMM. Therefore, the result will present two different calibrations continuously throughout the chapter. The old calibration method will be referred to as the base calibration, and the new method will be referred to as the work piece calibration.

First, calibration using the base as reference will be described, where the result of each measured point in xyz can be seen in figure 5.8. Here it can be observed that the deviation between the camera and the robot are less than in the experiment from Chapter 4. The reason for smaller deviation in the new experiment is simply that the workspace is smaller. Hence, it is easier to achieve smaller deviations since it exists less restrictions to obey. In figure 5.8, cal_1 and cal_2 are the two calibration points, located at the approach and withdraw point in figure 5.7. Therefore, the calibration for point 1 should be approximately equal for both cases, respectively for point 2 as well. In the y axis it is noticed that this is not the case, which will be discussed this further in section 5.3.

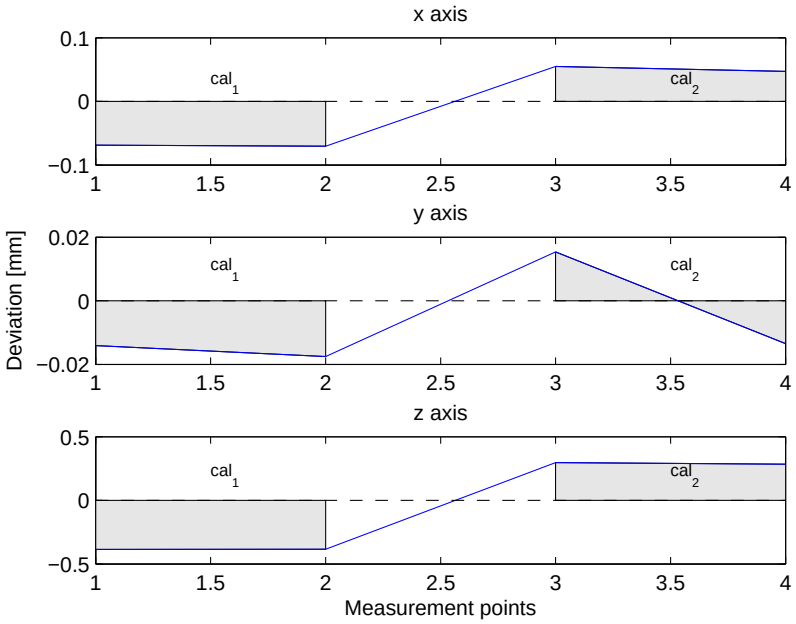

Figure 5.8: Calibration deviation in x, y and z when using the base as calibration reference.

For further analysis of the calibration, the 3D image of the calibration into three different planes is applied, notice figure 5.9. The color bar illustrates the measurement number. The figure confirms the observations from figure 5.8 from another perspective. From a 3D perspective view, it is difficult to achieve scientific conclusions of the calibration data, the deviations are more observable in a 2D perspective view. It is observed from figure 5.8 that the deviations are smallest in x and y axis, and large in z axis.

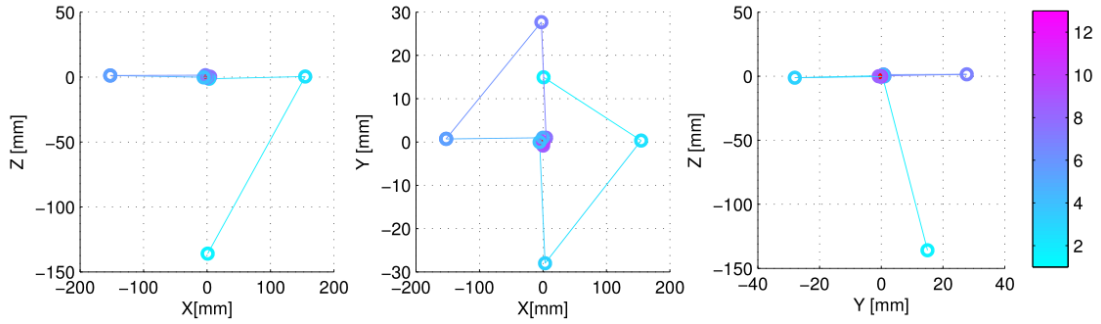

Figure 5.9: Calibration deviation xz, xy and yz plane for robot base. It consist of 13 measurements defined by the color bar, where not every measurement gave improvement.

By calculating the mean of the calibration points, the numerical differences can be seen, table 5.3. This table work as a supplement for figure 5.8 and 5.9. Figure 5.9 consist of 13 measurements to find a satisfying result. All the measurements are given in table 5.2, where the numerical progression throughout the measurements can be viewed.

Measurements	**x [mm]**	**y [mm]**	**z [mm]**
1	0.9457	14.9627	-135.9110
2	154.6573	0.3315	0.4497
3	3.3329	-28.0064	-1.2267
4	-5.2227	-0.0119	-0.2701
5	-0.0995	0.9747	-0.1969
6	-152.5190	0.7123	1.2156
7	-152.5036	0.7453	1.2364
8	-2.5009	27.7055	1.4318
9	5.0072	0.9880	0.3059
10	0.2689	-0.8234	-0.0591
11	-0.0423	-0.2852	-0.0645
12	-0.0629	-0.0673	-0.0574
13	0.0078	-0.0411	-0.0538

Table 5.2: Deviation between calibration point and the camera. The table is given to supply figure 5.9.

	Cal 1	**Cal 2**
x axis	-69.6 µm	51.0 µm
y axis	-15.8 µm	0.941 µm
z axis	-385 µm	290 µm

Table 5.3: Deviation between calibration point and the camera. Cal 1 and Cal 2 represents the mean of the two points from figure 5.8.

The measurements in table 5.2 are the mean values between the two calibration point, but the table is minimizing values on behalf of that it is wanted to produce the least deviation over the entire work piece. For some sequences in table 5.2, it is experienced some mistakes, which can be seen in measurement 6 and 7. After 13 measurements for the two calibration points it was achieved a deviation between the camera and the robot within 53.8 µm. By reviewing the camera capability, it has a precision of 60 µm in section 3.2.1.

For the work piece calibration there are 9 measurements given in table 5.4. The precision managed to reach within 18.8 µm as the mean between the two calibration points. The new respective plot for table 5.4 is given in figure 5.10. It can be observed that the measurements find a satisfactory calibration after 9 attempts.

Measurements	**x [mm]**	**y [mm]**	**z [mm]**
1	8.3718	-17.1178	2.1311
2	13.2080	1.3204	0.1307
3	0.5495	-2.5755	-0.2010
4	-0.4873	-0.2362	-0.0334
5	-0.0631	0.0860	0.0214
6	0.0093	0.0158	-0.0250
7	0.0406	0.0100	-0.0199
8	0.0372	0.0350	0.3176
9	-0.0041	0.0170	-0.0188

Table 5.4: Deviation between calibration point and the camera. The table supplies figure 5.10.

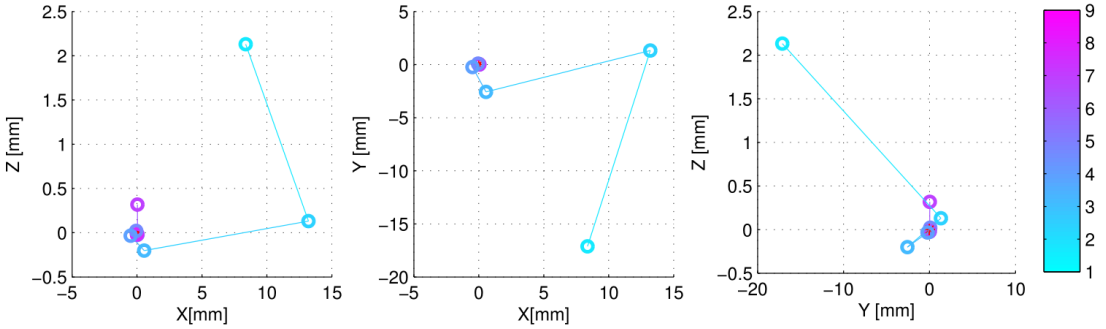

Figure 5.10: Calibration deviation xz, xy and yz plane for workpiece. With improved experience of the Optical CMM, advanced measurements are found more rapidly.

5.2.2 Force Control Measurements

To verify that the forces applied to the metal plate correspond to the output, the force signals from the TSV must be examined. The forces are applied in the force frame, which is defined identically to the tool frame in this experiment. This means that forces are applied downwards, which is the same as the positive z axis for the tool. Hence, the result will present positive forces with respect to the z axis. Figure 5.11 presents the results of the forces applied, which are 1 – 50 Newton of controlled pressure against the object. The figure shows the raw data and filtered data of the process.

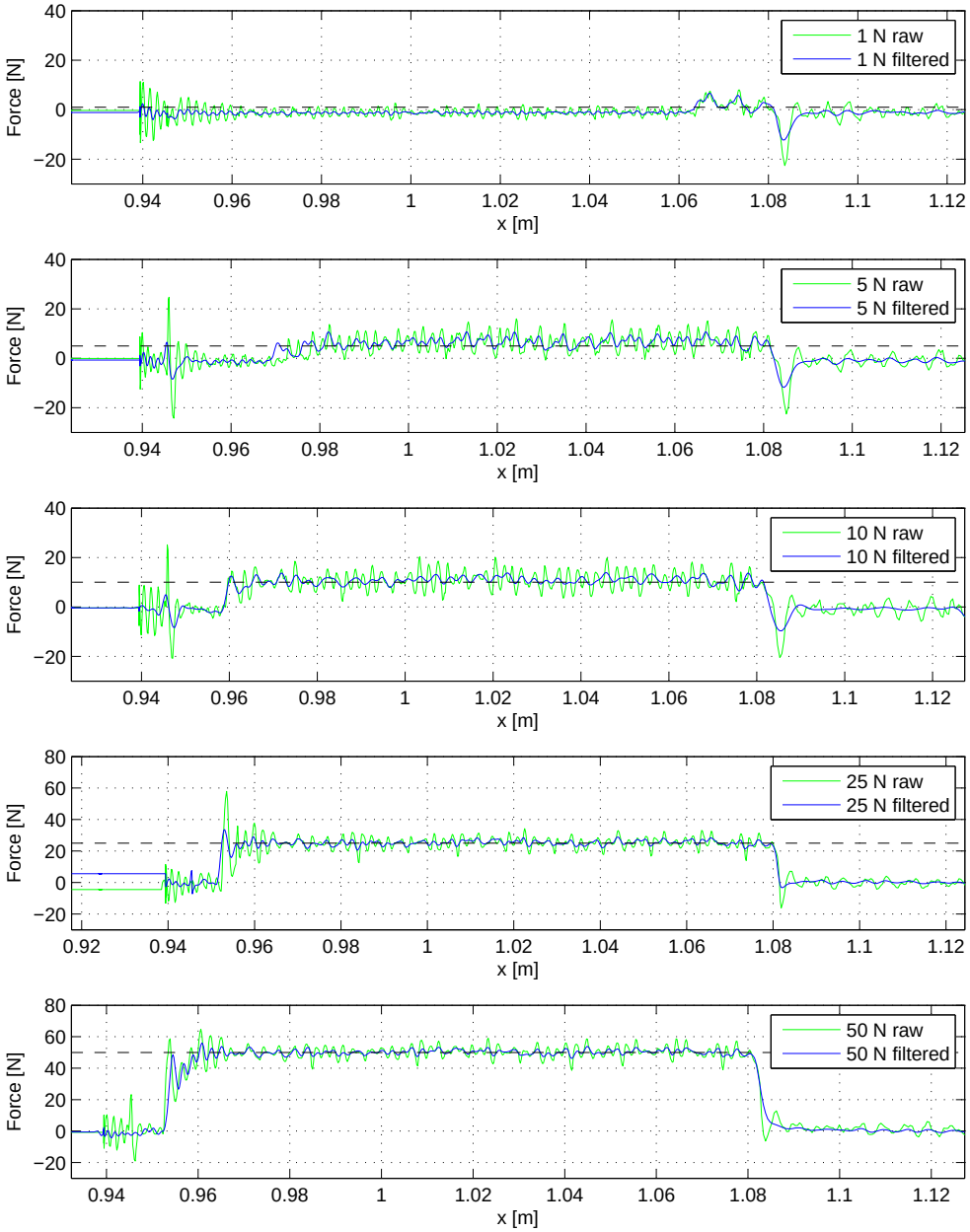

Figure 5.11: Different forces applied to the object. Notice that every force have different impact position until 25 Newton.

The filter is a low pass filter of 5 Hz that is applied in TSV. The reason for applying a filter of 5 Hz can be seen in figure 5.12. Here it can be observed that the force response contain high amplitude components of noise from 5 to 12 Hz. The behavior after filtering the signal can also be noticed in both figure 5.12 and 5.11, where the spikes of the raw force signal are removed.

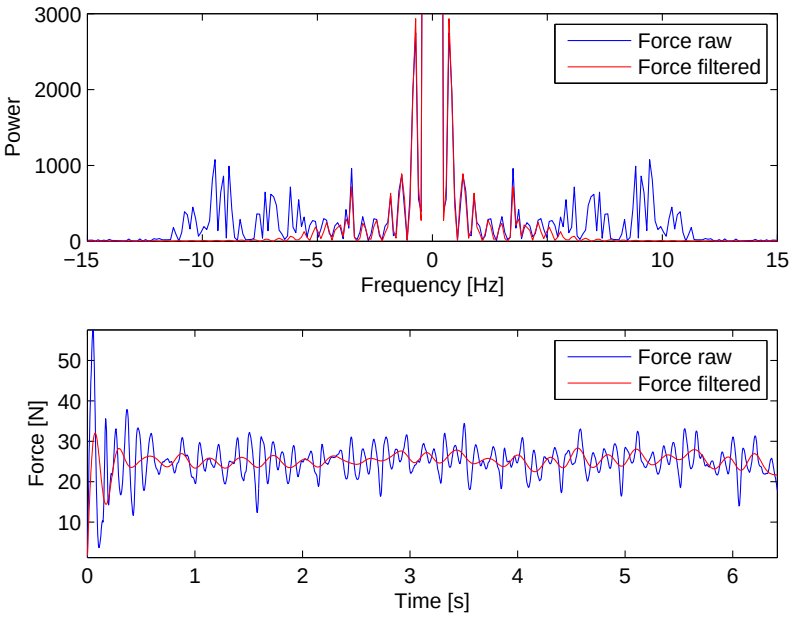

Figure 5.12: PSD with the noise components in the top and the respective force applied of 25 Newton in lower. Notice the effect of filtering with a 5 Hz low pass filter.

From figure 5.11 it can be observed that when 1 Newton is applied, the contact point is delayed till 1.06 meters. The reason for the undesired behavior is that the robot feels it way downwards as it proceed forwards since the force is less than 0.1 kg. Compared to the tool itself, which is approximately 45 kg, 1 Newton pressure is difficult to detect. The impact location is therefore later than programmed approach position. From earlier, the programmed impact position at 0.9485 m and the withdraw position at 1.0862 m along the x axis. To see whether the impact and withdraw moment are sufficient, notice table 5.5, which supplies figure 5.11. The table shows the measured impact and withdraw position and the calculated deviation from programmed impact and withdraw position. Also for 10 Newton

pressure, the impact moment is delayed by 1.05 cm. For 25 and 50 Newton the approach and withdraw point is approximately at the corresponding programmed path.

Force [N]	**Impact [m]**		**Withdraw [m]**	
	Position	Deviation	Position	Deviation
1	1.065	0.1165	1.082	0.0042
5	0.972	0.0235	1.083	0.0041
10	0.959	0.0105	1.083	0.0041
25	0.951	0.0025	1.083	0.0041
50	0.951	0.0025	1.083	0.0041

Table 5.5: Impact and withdraw position along programmed path. Notice that the impact position varies the most.

5.2.3 Velocity Observation

The velocity of the path is programmed equally for each test run. As mention, the programmed approach and process velocity is 20 mm/s, while the the programmed withdraw velocity is at 50 mm/s. From figure 5.13, the velocity is presented as a function of distance traveled, $\dot{x}(x) = c$. In the plot, the velocity is compared from the camera with the robot. The velocity is calculated by the derivative of the position of the robot. Hence, noise is experienced from the data. Notice that the velocities are sufficiently similar to programmed velocities.

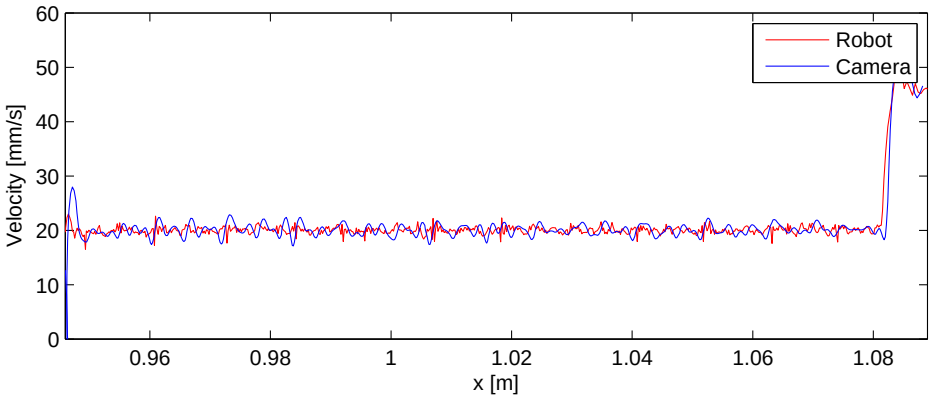

Figure 5.13: Velocity for for the process part. We can see from robot and filtered camera measurements that the velocity $\dot{x}(x)$ is similar for both cases.

5.2.4 Deviation Between Camera and Robot

In this section, it will be revealed whether measurements from robot encoders under processing are consistence with its actual position. The camera system measure with respect to the LEDs attached, and is therefore a reliable source for whether the end effector of the robot determine another position when applying different forces. Figure 5.14 presents the measurements from the robot position generated from the encoders, which is calculated using forward kinematics. The calibration is done in the base of the robot, as explained in section 5.1.2.

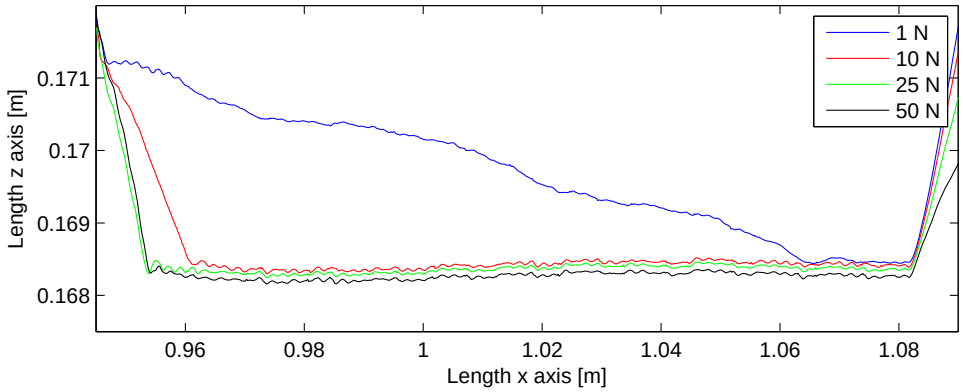

Figure 5.14: Robot position along the path when the base is used as calibration reference. Notice the displacement in z for the different forces.

From figure 5.14 it was observed that the position of the robot is separated in different layers in the z axis. The impact and withdraw position in table 5.5 also applies in figure 5.14.

The force of 1 Newton, is struggling to do an impact on the object. When 10, 25 and 50 Newton of controlled pressure force is applied, the measurements from the robot indicates that the tool tip is further down on the z axis when applying more force. In figure 5.15, it can be seen physical measurements from the camera system. The camera observe the behavior of the different forces similarly at every run. Thus, the displacement in the robot is only caused by robot measurements.

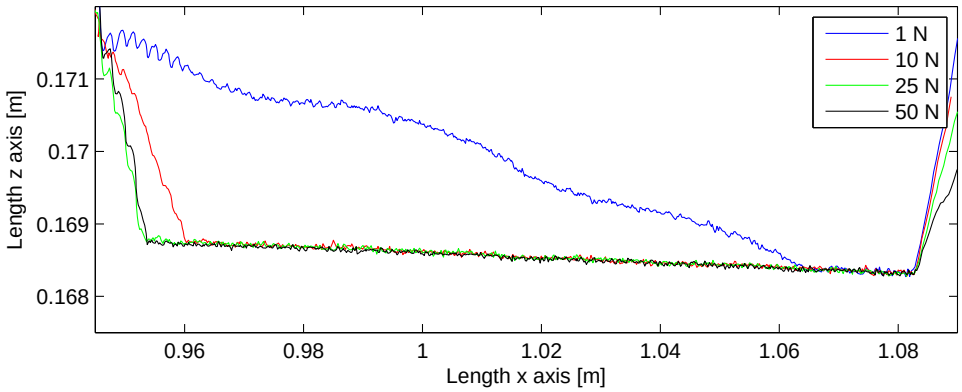

Figure 5.15: Camera position along the path when the base is used as calibration reference. Notice that the displacement does not physically existing, revealed by the camera measurements. Also notice the steepness of the measurements.

5.2.5 Work Piece as Calibration Reference

In this section the result of the procedure in 5.1.2 will be presented when the work piece was used as calibration reference. Additionally from the other FC experiments in this chapter, a force of 5 Newton is added to have a broader image of behaviors at minor forces. The result for the robot and camera measurements are presented in figure 5.16 and 5.17, respectively.

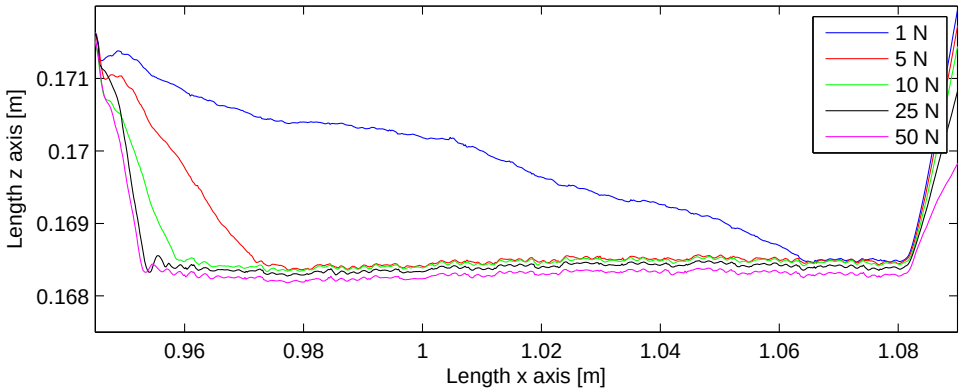

Figure 5.16: Robot position along the path when the work piece is used as calibration reference. The behavior is similar to what is observed in figure 5.14.

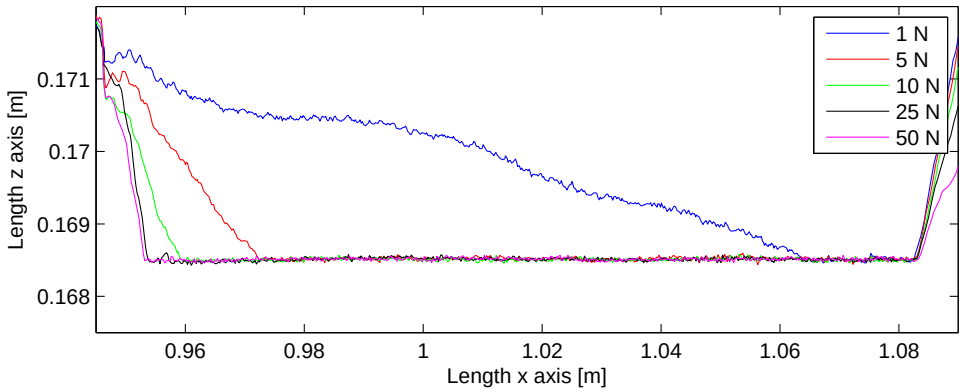

Figure 5.17: Camera position along the path when the work piece is used as calibration reference. Notice that the measurements are more leveled than in figure 5.15.

Because it is difficult to compare figure 5.16 and 5.17, it is desired to represent the measurements in the same plot. Figure 5.18 shows this representation. This figure shows forces from 5 to 50 Newton of the new calibration method. It can already be observed that the new method give more leveled measurements for the Optical CMM.

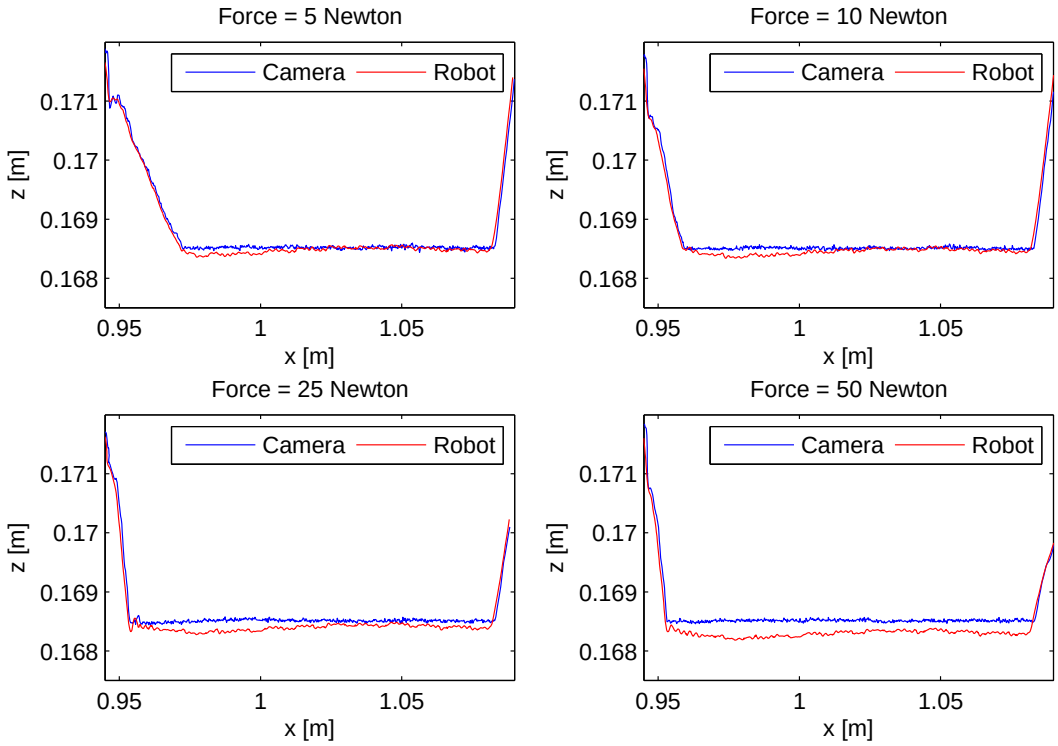

Figure 5.18: Camera versus robot for 5 to 50 Newton. Notice that camera measurements are horizontal and that the robot is displaced for larger forces.

From figure 5.18, the camera is leveled at 168.5 mm and the robot has displacements in z direction. This phenomena can be caused by collapsing links in the robot and will be deliberated more in section 5.3. Figure 5.19 represent the same experience, where the deviation between in camera and robot is presented. Here it can be seen that the deviation increases for larger forces. The measurements from section 5.2.4 could also confirm the displacement in z. The difference from section 5.2.4 is that the camera is more leveled with respect to the robot, see figure 5.18. The differences between the base as calibration reference and the work piece as calibration reference will be discussed in section 5.3.

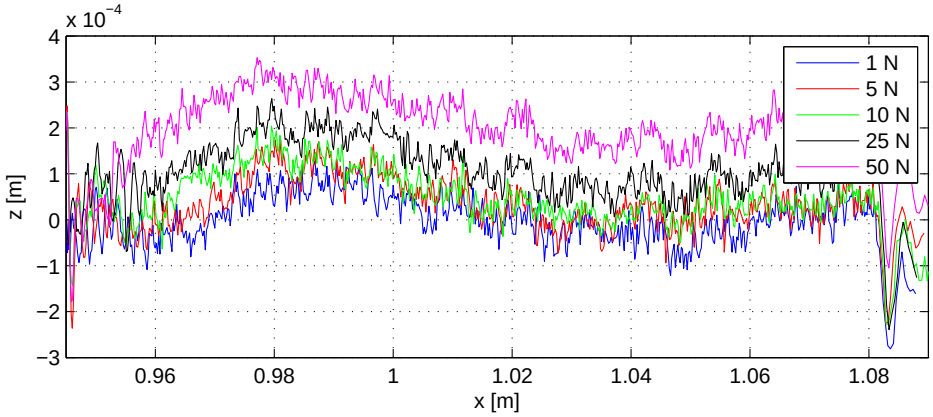

Figure 5.19: Deviation between camera and robot position for 1 to 50 Newton. Observe the oscillating behavior, which comes from the robot measurements. These are unwanted behaviors that acquire compensations to have improved quality of future products.

5.3 Discussion

This section discuss issues that have been brought up during the results. First, the designed tool will be examined, whether it has potential for improvements, then the characteristics for the displacement of the robot when the links are collapsing will be studied and to research its behavior when applying FC, and lastly, frequency components will be studied for the FC experiments.

Tool Design

The tool developed to accomplish the experiment with FC, was designed to go along linear trajectories, see figure 5.4. The wheel is static without the ability to rotate, which means that there are experienced more friction forces if the wheel is not aligned with the path. As the attachment location for the rod itself can rotate, it is possible to get out of position. Therefore, another way of designing the tool must be considered.

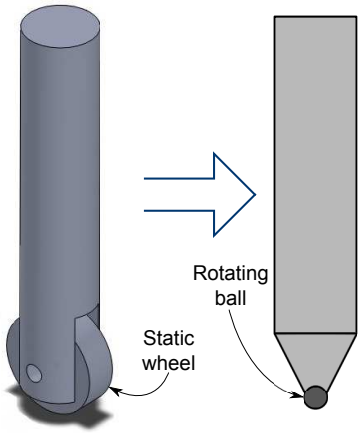

Figure 5.20: Modified tool which replaces the static wheel with a rotating ball.

An alternative is shown in figure 5.20, which is improved with the design of a pen. The design let the end effector go along any direction while in contact with an object. This is a more complex tool design than the tool in figure 5.1. On the other hand, the tool with a wheel can come out as leading when it comes to rigidness. The fragile part is the bolt stuck in the wheel or the wheel itself. The benefit of a more rigid tool is that more forces can be applied without breaking it.

Base Versus Work Piece as Calibration Reference

A major part of the experiments presented in this report, utilize the robot base as calibration reference to create the dynamic base of the camera system. The problem with using the base as calibration reference is that the robot base tend to tilt towards the center of mass.

In section 5.2.5, the calibration reference was changed from the base on the robot to a plane defined on the metal piece. Then the comparison between the camera and the robot was more leveled to each other in the small workspace operated in.

If the work piece is perfectly leveled with a leveling tool, the dynamic base defining the robot will also be perfectly leveled as the dynamic frame is shifted towards the origin o_0 of the robot, see figure 5.2.

As deviation in z along the direction x of the object is measured, the normal from the object should be approximately parallel to the z axis for the robot. By reason of the object is approximately planar, parallelism is achievable and it can be view from position measurements $x(z)$ in figure 5.18, that the z axis has improved its level from $x(z)$ in figure 5.15, where the robot base was used as calibration reference. By comparing the robot base and the work piece defining the planar dynamic frame, it can be observed from figure 5.21 that the performance was improved.

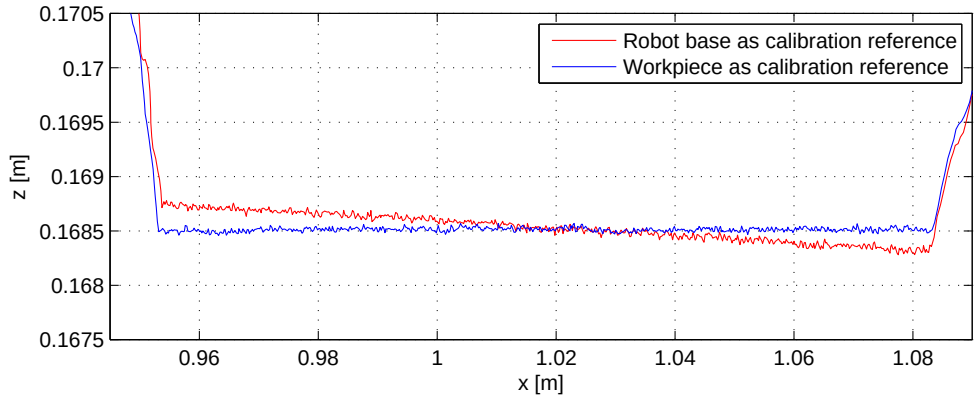

Figure 5.21: Comparing calibration for the dynamic base of the camera. Notice that the performance is approximately leveled for the work piece as calibration reference.

The work piece as calibration reference for $x(z)$ is approximately leveled. For the robot base as calibration reference, a tilt in y is measured, possessing a slack descent of $0.0031°$. The descent is not within satisfactory limits, and therefore the work piece is a more suitable location to define the dynamic frame. This may also be proven by calculating the least absolute deviation away from the reference $z = 168.5$ mm, the $\mathcal{L}_1$ norm. Thus, the deviation when in contact with the metal object is found to be

$$||z||_{1,\text{Base}} = 0.231, \qquad ||z||_{1,\text{Workpiece}} = 5.61 \times 10^{-4}. \tag{5.1}$$

The deviation using the the base as calibration reference is proven in equation 5.1 to be approximately 41 times larger than the work piece as calibration reference. Thus, the work piece should be a clear choice for future experiments when developing horizontal and dynamic frames for the camera.

Collapsing Links of the IRB 4600

As noticed from figure 5.14 and 5.16, the robot have a displacement in the z axis for different forces. By studying this observation further, an approximation of the displacement can be made. By comparing the displacement in z with the force

applied, the tendency of how force affect the displacement in z can be observed. From this comparison, it can be seen from figure 5.22, that the plot has the characteristics of a first order polynomial, which is:

$$h(Force) = 2.1861 \times 10^5 e + \sigma, \tag{5.2}$$

where σ is the standard deviation of the force measurements and is calculated to be $\sigma = \pm 3.6$. The force is calculated as a function of the error e along the process when FC is active. From figure 5.14 it can be observed that the displacement in z is not consistent. Hence, the input data of the mean calculations in figure 5.22 is not perfectly fitted.

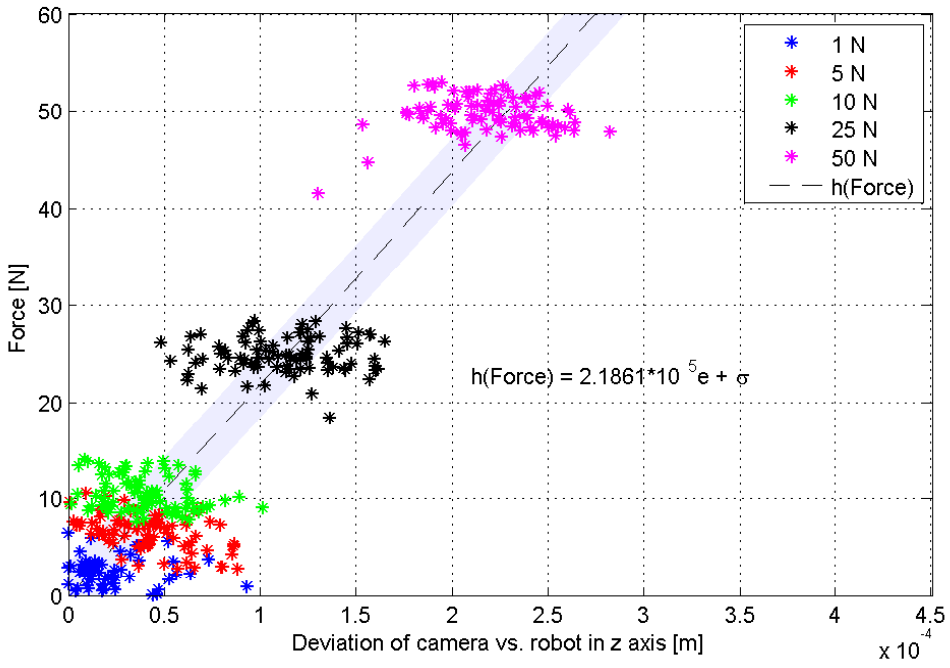

Figure 5.22: First order function of force versus displacement in z. A 5 Hz low pass filter in TSV filters the forces.

A subsidiary goal of the experiment was to reveal dynamics with the Optical CMM for the IRB 4600. It was seen from the displacement in figure 5.14 and 5.15 that the measurements deviate when forces are applied. Several facts can be established from figure 5.15:

- The forces applied in the process is proofed to be at the same level by the camera measurements. Thus, it can be confirmed that the robot is actually mistaken by the length given by the function in figure 5.22 when FC is applied for the given scenario.
- The length along z for the camera system is not consistently leveled with the robot measurements. The reason for unleveled measurements is due the facts discussed in previous experiment in section 4.3, that the base of the camera is inaccurately calibrated. Because of unleveled measurements, it was compensated by using the work piece as an object to define the planar xy of the frame. The outcome was a major improvement obtaining leveled frames between the camera and robot, which was seen in figure 5.21 and equation 5.1.
- The camera measurements carry minor noise components, which is a indication of well placed LEDs with respect to width and depth.

Researching Frequencies Components

A topic of research is to examine the frequency components of the measured signals. It is desired to compensate for frequencies, which can result in a product of higher quality. The signals for force and position at the end effector have oscillations, which can be corresponding to each other. By looking into the signals, the behaviors in figure 5.23 can be observed, which has a force applied of 25 Newton.

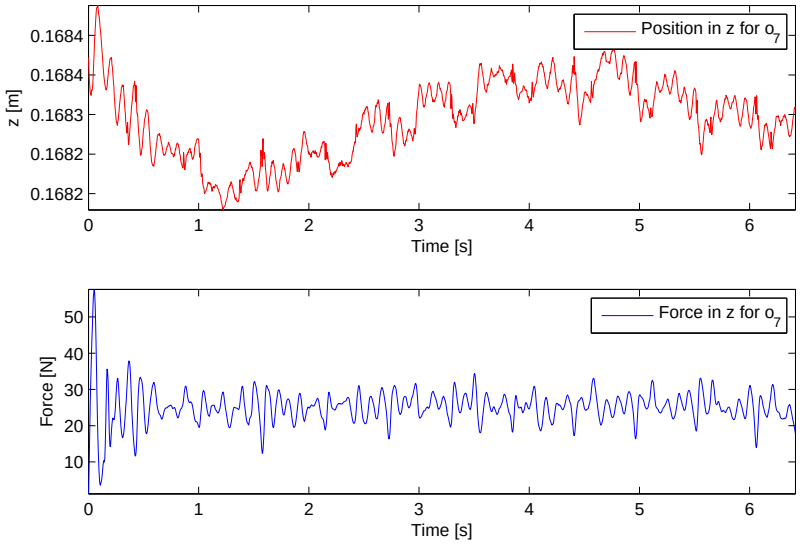

Figure 5.23: Force in lower figure and position in top figure for processing with 25 Newton force along the metal object.

The signals seem at first to have some similar frequency components, which will be studied further in the power spectrum plot in figure 5.24. It can be observed that the dominant frequencies in the force measurements have the same structure as the frequencies for the measurements of the encoders giving the position of the tool. To see similarity however, the measurements of the position is scaled up by a factor of 2×10^4. Otherwise, a comparison study is more difficult to obtain. To view the whole power spectrum of the force, observe figure 5.12 in section 5.2.2.

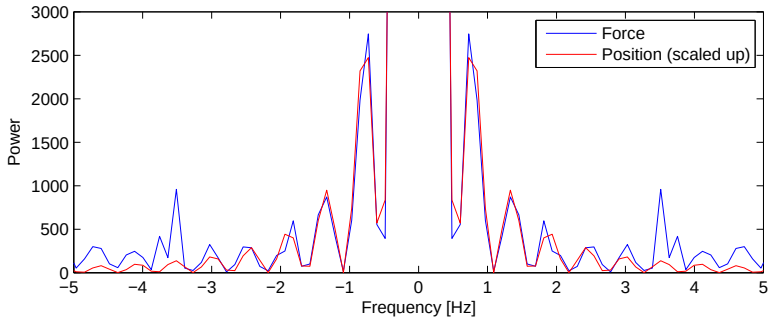

Figure 5.24: PSD with 25 Newton force. The position measurements are scaled up to be able to compare with force measurements.

Whether the dominant frequencies of the position are obtained by FC, can be verified by comparing frequencies from trajectory performances in Chapter 4. In figure 5.25, a time series in z can be observed. The series is a trajectory without processing from figure 4.5, while motions only apply in x direction with respect to the robot base. It can also be observed a time series when FC is applied. The trajectory of non-processing have frequency components which can be compared to the FC part.

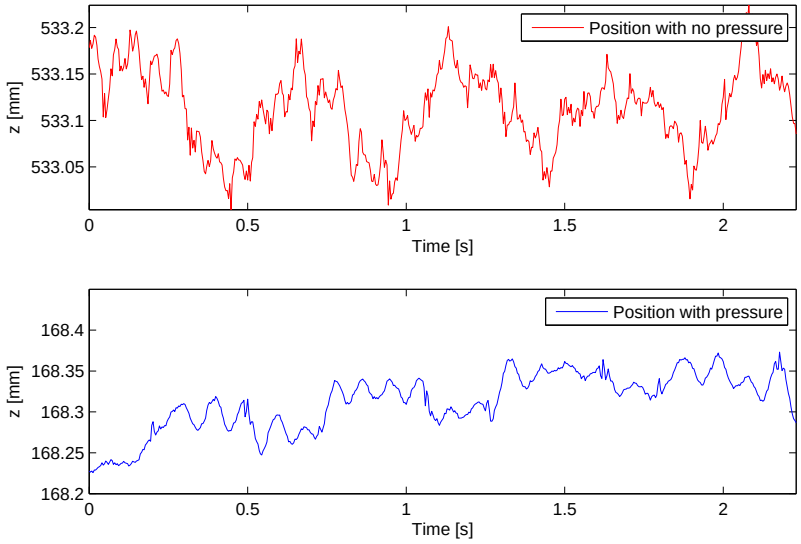

Figure 5.25: Comparing robot position with and without FC. The measurements are picked out from a chosen time series, where both have motions only in x with respect to the TCP.

Another observation that can be done from figure 5.25, is that the amplitude of the frequencies when applying FC is smaller than without FC. For the trajectory without pressure, the peak-to-peak amplitude is approximately 200 µm, while with pressure it is 100 µm. Hence, the position measurements tend to be less noisy when the wheel tool is in contact with the object surface.

Less noise for FC may not always be the case when performing a grinding or polishing process of the object. Then vibrations of the drill tool will create noise, which is of higher scale than when having a movement without contact of an object.

The PSD of the comparison in figure 5.26, shows that the frequency components while FC is applied, are similar as when FC is not applied. Thus, the dominant frequency components for the position do not occur as FC is applied. The frequencies already exists in the end effector while performing motions. As observed from 5.12 however, there are frequencies that can be compensated which do not occur for the position. However, the FC scenario generate slow oscillations which are part of the DC component. Thus, there exists opportunities of improving the performance.

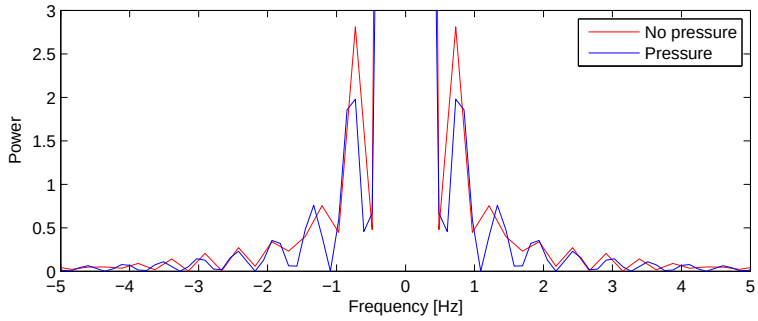

Figure 5.26: Comparing power spectrum with and without FC. Observe that frequencies over 0.7 Hz already exists in the signal without using FC.

Movement of the Robot Base

The IRB 4600 stands on a track which can move sideways along y with respect to o_0 of the robot. The track, called an IRBT 4004, is not completely static, notice the robot on the track in figure 1.1. It is known that the base moves or tilt sideways along the center of mass of the robot. As movement in the base is undesired, the movement is examined from the LEDs attached to the base.

The LED measurements is plotted in figure 5.27. The figure contains history of data, where the color bar describes the time. The color bar is ranged from 0 to 1, which means the time from t_0 to t_{end}, respectively. From the figure, it is noticed that the LEDs do not observe any movement of the robot base, by viewing the small scaled axes.

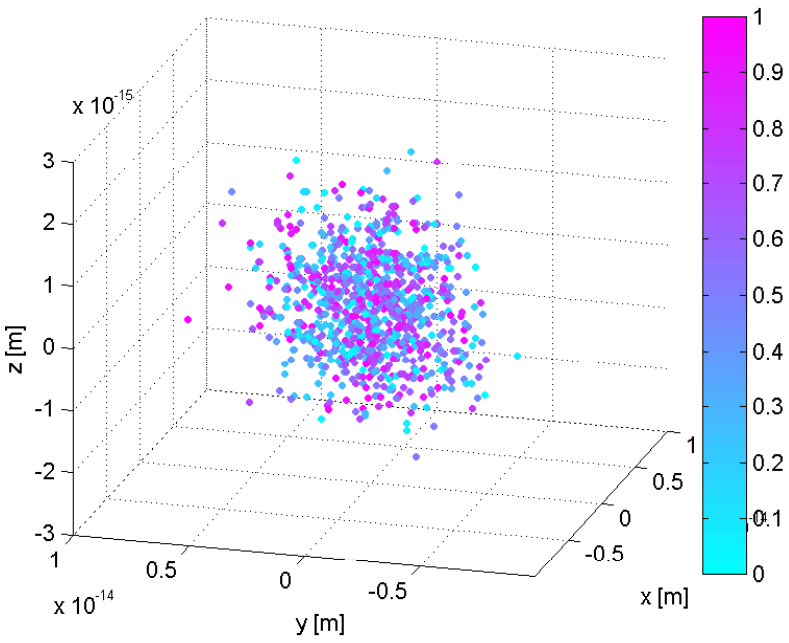

Figure 5.27: Measuring dynamic base of the camera. The color bar represents the history of data from time start to end.

The static behavior may come as a reason of several factors, whereas LED placement may cause the behavior. The force applied in the process is 50 Newton, but the base behave in a similar pattern for minor forces as well. Thus, it cannot be confirmed that the base actually moves. There exists two possible explanations why movements cannot be detected in the base, which is the LED placement and the method of calibration:

(i) Since the LEDs are attached at the edge of the base, the LEDs cannot see movement because the edge of the base is not moving. The movement is greatest in the center of the plate, i.e. the robot base o_0. If LEDs were placed towards the center, the movement could be identified. This is however, hard to achieve because there are limited space of attachment on the base, which could give the desired measurements.

(ii) The calibration of the robot was done when the robot was lending towards its workspace, such that the center of mass was already shifted when calibration

was performed. Thus, when the camera system captures the reference of the LEDs, the robot base is already tilted. When motions are performed in the already tilted base, it cannot be detected if the base has tilted since the measurements operate in a tilted robot base space. Thus, the robot requires to be calibrated such that the center of mass is straight above o_0, then the base should be leveled.

It is applied 50 Newton force in figure 5.27, but a force of 5 kg is small when the robot itself weight approximately 400 kg. However, it should be seen some motions when the force is active in figure 5.27. Therefore, a combination of LED placement and the calibration method affects the results such that movement in the base cannot be detected from the Optical CMM.

Experimentations shows that the base tend to tilt towards the mass center, dependent on where the robot lean towards. The behavior is illustrated in figure 5.28, where red lines depict the theoretical position of the robot, i.e. where the robot think it is on behalf of the robot base. Black lines illustrates the physical robot behavior, i.e. the motions captured by the camera system.

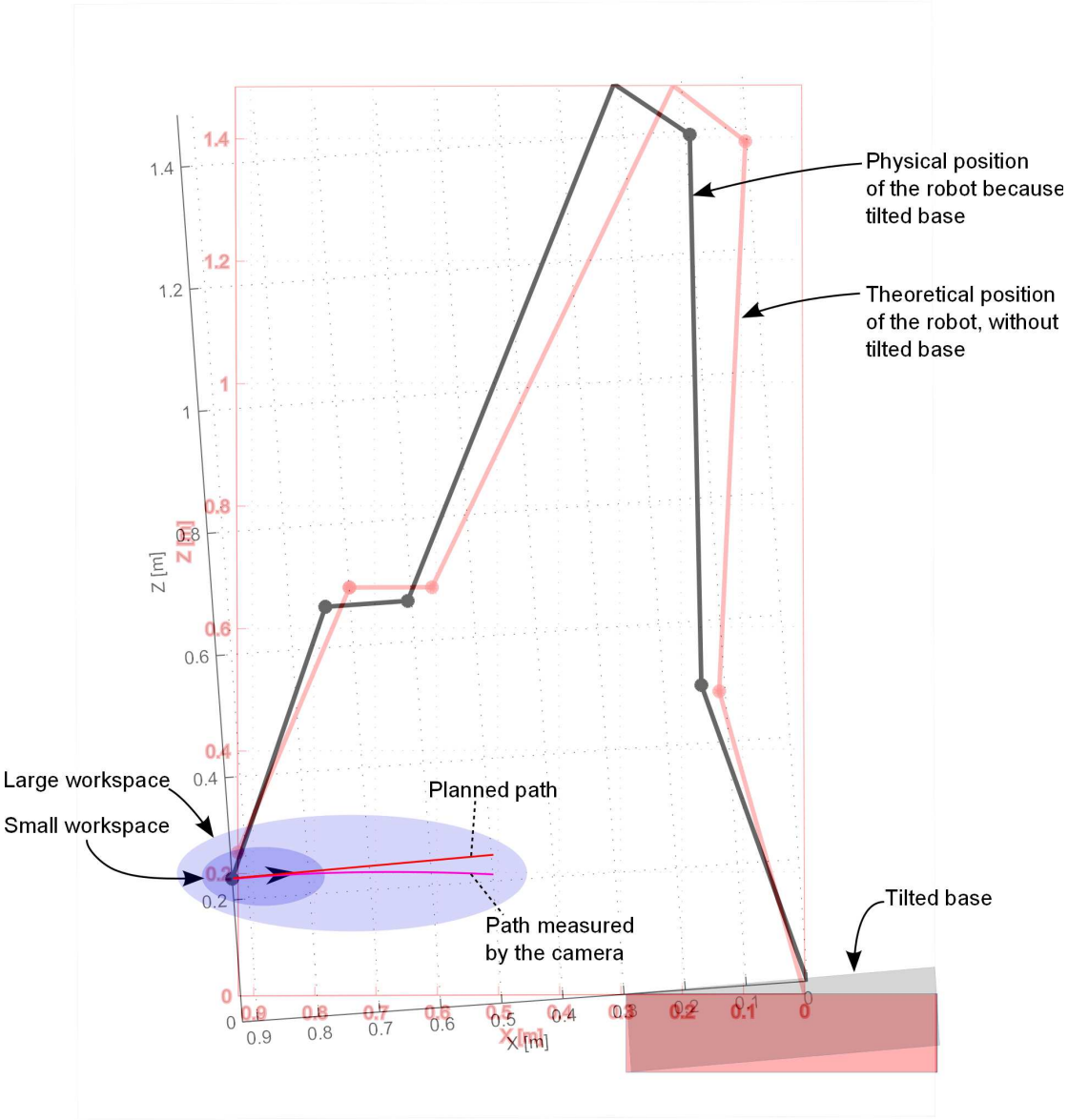

Figure 5.28: Tilting base disturbs measurements. When the base moves, the path measured by the camera is not consistent with the robot measurements for a large workspace.

The robot encoders track the position of the end effector by joint calculations without concerning if the base is tilted. The camera system should also, in theory if LEDs were placed optimally, track the end effector the same way as the robot

encoders, because the LEDs attached to the robot base should be moving with the base. Since the robot base tend not to move, from the current LED location, the behavior of a path will bend along with the center of mass of the robot. From figure 5.28 the curved and linear path can be seen, where planned path and the same path measured by the camera is illustrated.

The black coordinate frame is tilted because of the tilt in the robot base. The illustrated paths are based on results in figure 4.11 and 5.21. Since the base are moving with the center of mass of the robot, the paths tend to have a form of second order function as shown in figure 5.29. It is important to notice that the behavior of the path is nonlinear only when observing camera measurements or when comparing the camera with the robot.

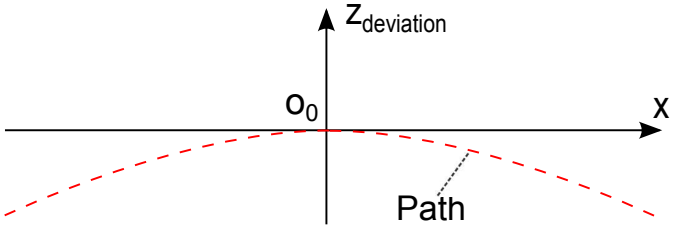

Figure 5.29: Tendency of the path because of the behavior of the base. Since it is assumed that the base moves, the camera will capture this kind of behavior.

For most cases it will not be possible to see the entire path illustrated in figure 5.29, only to observe the path in a certain workspace as in figure 5.28. By studying the workspace in figure 5.28, the tendency of a second order functions weakens when the workspace is smaller versus a larger workspace. This fact is also recognized from figure 5.21, where both the base and the work piece calibration tend to be linear. Therefore, the angle calculated to be 0.0031° for the robot base only applies for a small workspace along the planar space. More specific, the calculated angle applies when x is between 0.96 and 1.08 meters.

Till now, it has only been mentioned the base as a reason for the behavior illustrated in figure 5.29. There could be several more factors, other than the base displacement, that affects this behavior. One other dominant aspect is collapsing links and arms of the robot. Since gravitational forces are affect the performance, collapsing links and arms are experienced when the robot is located further away

from its origin o_0. The sum of displacement of the base and collapsing links and arms of the robot creates the behavior recognized in figure 5.28.

As can be seen from figure 5.16, a displacement in the end effector calculations was observed, even though it is known that collapsing links of the robot are causing the displacement. Regardless of the robot, the tool designed in section 5.1.1 must be considered as it may also collapse. Collapsing tool can create undesired behaviors such that we lose dynamics.

The wheel movement in z for the tool was approximately measured within microns, i.e. the slack of the wheel. Even though, if the displacement were up to one millimeter, the dynamics would still be intact for the robot. The reason for this is that once contact is established with the metal object, the dynamics of the tool has disappeared.

The tool has gone from slack in the wheel to a rigid component as contact with the object is settled. Thus, lost motions because of the slack in the wheel is unlikely, it remains static and rigid when force is applied to the object.

Alternative Methods for Applying Velocity

In figure 5.19, it does not only occur displacement in z, but also a form of oscillations. From the graph in figure 5.19, the slow oscillations have one period along the path while in contact with the object. The path is completed in seven seconds, which means the oscillations is approximately 0.14 Hz. The oscillation is too slow to be seen in the power spectrum in figure 5.24, and come out as part of the DC component of the spectrum.

The goal is to compensate for these oscillations, which are present for every event when FC is applied. There exists untried methods that can give more understanding of the oscillating behavior. The objective of the thesis is to study such behavior and to propose compensating methods. When its behavior is understood, controllers can be designed to compensate for the oscillations.

For the experiment presented in this chapter, the same constant velocity was applied to the end effector while in contact with the object. An option could be to

apply other velocities as well to see if the oscillations remains the same. The plot of velocity can be seen in figure 5.13, where the derivative of the position for the end effector was calculated for both the camera and robot.

There also exists alternative procedures to apply the velocity. In this experiment, constant velocity is applied and has the function $x(t) = c$, where c is the constant of arbitrary choice within reasonable limitations. Another straightforward implementation could be to change velocity during the FC performance. Two different alternatives is then possible.

(i) The first is to implement a step based velocity, which change velocity $\dot{x}$ several times during the time pressure against the object is active. In this way it can be observed whether the oscillations change form for each step, and a compensation could be accomplished by setting optimized step based velocities at some distance x along the object. In other words, $\dot{x}(x) = h(x)$, where $h(x)$ is the step based function.

(ii) The second option is to implement the velocity as a polynomial along the path. The polynomial can be a sum of coefficients which is optimized such that the velocity changes during the path as a function of the distance x. By producing a number of experiments applying the velocity polynomial, this may be a more improved way of compensating for the oscillations in figure 5.19 completely. The polynomial can have the form

$$\dot{x}(x) = \sum_{i=0}^{N} a_i x^i = a_0 + a_1 x + a_2 x^2 + \cdots + a_i x^i, \tag{5.3}$$

where N is the order number of the polynomial and a_i is the preferred coefficients.

The three methods mentioned for velocity implementation, are summarized in table 5.6 and illustrated in figure 5.30.

	Method	Function	Status
1	Constant velocity	$x(t) = c$	Tested
2	Step based velocity	$\dot{x}(x) = h(x)$	Untested
3	Polynomial velocity	$\dot{x}(x) = \sum_{i=0}^{N} a_i x^i$	Untested

Table 5.6: Tests of velocities accomplished and proposal for further test procedure when FC is applied.

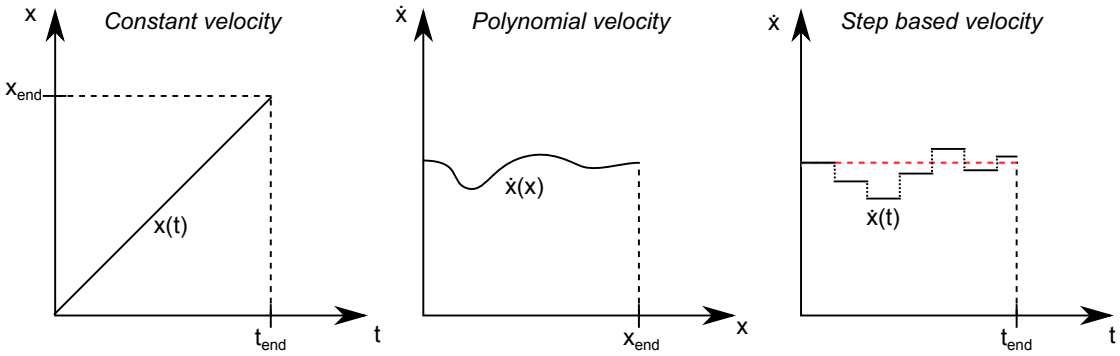

Figure 5.30: Methods of adjusting velocity during FC. The different methods can be the solution to compensate for the oscillating behavior in figure 5.19.

Statistics of the Calibration

Observation and experience of the camera shows that measurements with the Space Probe can be inaccurately. Therefore, a sequence of Space Probe measurements was repeated six times to observe tendency and robustness of the calibration. The Space Probe measurements follows the sequence in subsection 3.2.4, i.e. the base was used as calibration reference for the dynamic frame.

The rough surface that the robot stands on will be analyzed whether it is sufficient as calibration point. The result is presented in figure 5.31, where six calibrations are repeated from scratch and compared to one run of the robot when 25 Newton is applied to the object of planned path.

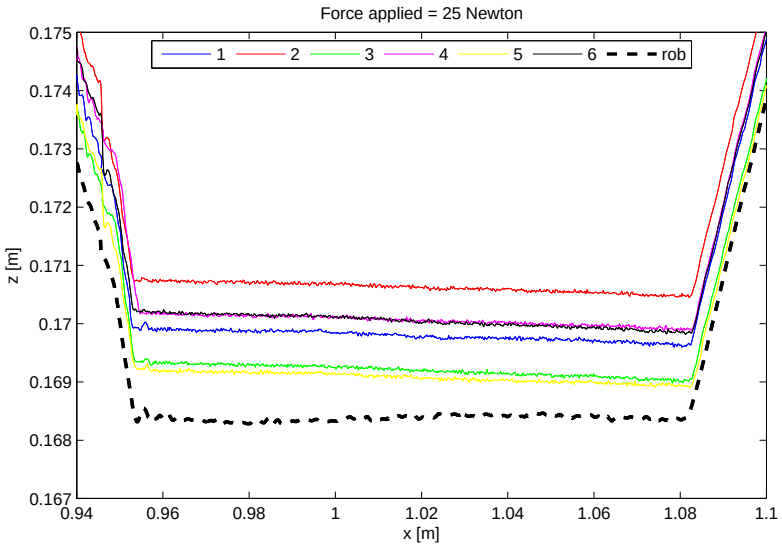

Figure 5.31: Statistic behavior of Space Probe measuring. Because of the rough plate on the robot base, the measurements have stochastic behavior. The descent observed is however, the same for each test.

The result shows a standard deviation of approximately 2 mm for the camera measurements. The camera measurements are also shifted approximately 1–3 mm from the robot encoders data. It must be taken into account however, that 25 Newton was applied, and that the robot is shifted more because of the force.

In this part of the thesis, all relevant work is presented. The remaining chapter will provide a conclusion for the entire thesis, attempting to sum up the achievements and to recommend future work of the FC topic.

CHAPTER 6

Concluding Remarks

The work in this thesis have been to plan, develop and analyze one of the complex scenarios for robots, which can be used for factories in the future. Measurements from the experiments were analyzed by comparing data from the camera system, the robot encoders and the FC signals. The case study have been split into two main test scenarios, which are motion study when the end effector moves freely in space, and motions while in contact with an object applying FC. The following paragraphs will conclude the experiences and results achieved from the experiments.

The calibration of the camera system is a time consuming process, since it is desired that the dynamic frame of the camera should map the end effector frame of the IRB 4600. Precision of the camera proves to be robust and repeatable, but it contained some noise if LEDs were not attached sufficiently with respect to height and depth. As seen from the first experiment, the challenge with the camera system is to map it to the end effector from robot measurements, globally. In a small space, the deviation between the camera and the robot can be fitted within 60 microns. When operating in a large workspace, the deviations drift off the further away from the calibration point the end effector is located.

For a major part of the experiments, it was challenging finding a satisfying defined dynamic base for the camera system. Improvements came when changing from the robot base as calibration for the xy plane to using the work piece as calibration reference defining the horizontal plane. Then it was accomplished a leveled comparison between the camera system and the robot. Moreover, with the robot base as calibration reference, results showed a rotation of $y_{rot} \approx 0.0031^\circ$ for the camera

system versus the robot encoders, and $y_{rot} \approx 0°$ for the work piece as calibration reference.

When FC was applied with forces from 1 to 50 Newton, a displacement for robot measurement could be observed which increased linearly with the force. With more force, a greater displacement was experienced which increased with the function $h(Force) = 2.1861 \times 10^5 e + \sigma$. Mostly, for 50 Newton FC the displacement reached approximately 240 µm, which gives $h(Force) \approx 52.5$ Newton for the linear approximation. The camera system revealed, by physical measurements that the displacement is not existing and it is therefore concluded that the displacement is caused by collapsing links and arms of the robot.

As observed from the robot measurements with FC, the position had a slow oscillating behavior of approximately 0.14 Hz during FC performances. This a behavior it is desired to compensate for in order to have improved quality for machining processes in the future. The experiments in this thesis had a velocity of 20 mm/s while in contact with the object. A theory is to change velocity with time to observe if the oscillations improves. If improvements are achieved, controllers can be created to compensate for the unwanted behavior. Thus, the proposal is to implement the velocity as a step based function with time or by developing a polynomial that changes with the distance traveled along the object. Further researching of the velocity would be the first step in order to understand the behaviors presented in this thesis. Because force must be constant in order to maintain quality.

The thesis has presented work concerning FC scenarios and developed a new tool to make experiments feasible. It was also found undesired behaviors and presented opportunities of compensations. For future experiments, there are still a great collection of researching topics. The first step would be to do experiments with different velocities, which was provided in this thesis. When compensations are developed, simulated and analyzed, the next step would be to develop controllers that can accomplish a flawless and quality strong result when grinding and polishing a chosen object. The final step would be to use a scanner from Nikon Metrology to observe if the product has improved quality between the experiments.

Bibliography

[1] ABB. *Application manual, Force Control for Machining*, 2009.

[2] ABB. *Product Manual IRB 4600*, 2009.

[3] ABB. *Function Package IRB 4600, Force Control for Machining*, 2010.

[4] ABB. *Test Signal Viewer*, 2013.

[5] P. A.Ioannou and J. Sun. *Robust Adaptive Control*. Courier Corpration, 2012.

[6] Y. Chen and F. Dong. Robot machining: recent development and future research issues. *The International Journal of Advanced Manufacturing Technology*, 66(9-12):1489–1497, 2013. ISSN 0268-3768. doi: 10.1007/s00170-012-4433-4. URL http://dx.doi.org/10.1007/s00170-012-4433-4.

[7] J. Fiene. Denavit-hartenberg parameters. MEAM Department, SEAS, University of Pennsylvania, 2012. URL http://medesign.seas.upenn.edu/uploads/Courses/robotics06dh.pdf.

[8] H. Kazerooni and M. Her. Robotic deburring of two dimensional parts with unknown geometry. In *Intelligent Control, 1988. Proceedings., IEEE International Symposium on*, pages 459–464, Aug 1988. doi: 10.1109/ISIC.1988.65475.

[9] T. Kroeger. Force control, 2015. URL http://cs.stanford.edu/people/tkr/research/force-control.

[10] B. Malone. A life devoted to invention, and robots, 2015. URL http://spectrum.ieee.org/automaton/robotics/industrial-robots/george-devol-a-life-devoted-to-invention-and-robots.

[11] M. T. Mason. Compliance and force control for computer controlled manipu-

lators. *Systems, Man and Cybernetics, IEEE Transactions on*, 11(6):418–432, June 1981. ISSN 0018-9472. doi: 10.1109/TSMC.1981.4308708.

[12] Nikon. K-series optical cmm, 2015. URL `http://www.nikonmetrology.com/en_EU/Products/Portable-Measuring/Optical-CMM/K-Series-Optical-CMM`.

[13] Nikon Metrology NV. *Introduction to Frames*, 2015.

[14] Nikon Metrology NV. *K-Series Optical CMM solutions*, 2015.

[15] Nikon Metrology NV. *K-Series Training*, 2015.

[16] Nikon Metrology NV. *LED Placement Guide*, 2015.

[17] J. G. Proakis and D. K. Manolakis. *Digital Signal Processing, Fourth Edition*. Pearson Education Limited, 2014.

[18] Robotiq. Robot end effector: Definition and examples, 2014. URL `http://blog.robotiq.com/bid/53266/Robot-End-Effector-Definition-and-Examples`.

[19] B. Siciliano and L. Villani. *Robust Adaptive Control*. Kluwer Academic Publishers, 1999.

[20] M. W. Spong, S. Hutchinson, and M. Vidyasagar. *Robot Modeling and Control*. John Wiley and Sons, Inc, 2006.

[21] W. Storr. Butterworth filter design, May 2015. URL `http://www.electronics-tutorials.ws/filter/filter_8.html`.

[22] The Music Zoo. Factory tour: Inside martin guitars, 2015. URL `http://www.themusiczoo.com/blog/2010/factory-tour-inside-martin-guitars/2/`.

[23] H. Zhang, H. Chen, N. Xi, G. Zhang, and J. He. On-line path generation for robotic deburring of cast aluminum wheels. In *Intelligent Robots and Systems, 2006 IEEE/RSJ International Conference on*, pages 2400–2405, Oct 2006. doi: 10.1109/IROS.2006.281679.

Appendices

Acronyms

DC	Direct Current
DH	Denavit-Hartenberg
DOF	Degrees Of Freedom
FC	Force Control
FSH	Focus Scan HandHeld
HMI	Human Machine Interface
IRB 4600	ABBs Industrial Robot 4600
K-Ref Bar	Measurement Device that comes with the K610 Optical CMM
LED	Light Emitted Diode
PDS	Power Spectral Density
Space Probe	Measurement Device that comes with the K610 Optical CMM
TSV	Test Signal Viewer
TCP	Tool Center Point

Example Code of Force Control

```
1  PROC RunPathFC (bool bRecover, bool bSpindleOn)
2      FCDeact;
3
4      IF bRecover = true THEN
5          FCCalib  toolMiller_LD \Recovery;
6      ELSE
7          FCCalib  toolMiller_LD;
8      ENDIF
9
10     IF bSpindleOn = true THEN
11         SpindleOn;
12     ENDIF
13
14     MoveL T1Approach1, v20, z1,toolMiller\wobj :=wobj0;
15     MoveL T1Approach2, v20, z1,toolMiller\wobj :=wobj0;
16     MoveL T1Approach3, v20, fine,toolMiller\wobj :=wobj0;
17
18     FCPress1LStart T1Process1, v20 \Fx:= n1ForceX \Fy:= ...
           n1ForceY \Fz:= n1ForceZ,50 ...
           \ForceFrameRef:=FC_REFFRAME_TOOL \ForceChange:=50 ...
           \DampingTune:=100 \TimeOut:=5, \UseSpdFFW, ...
           \PosSupvDist:=20, z1, toolMiller \wobj:=wobj0;
19
20     FCPressL T1Process2, v20, 10, z1, toolMiller, \wobj:=wobj0;
21     FCPressL T1Process3, v20, 10, z1, toolMiller, \wobj:=wobj0;
22
23     FCPressLEnd T1Withdraw1,v50,\ForceChange ...
           :=50,\ZeroContactValue := 5;
24     MoveL T1Withdraw2, v50, z1,toolMiller\wobj :=wobj0;
25
26     IF bSpindleOn = true THEN
27         SpindleOff;
28     ENDIF
29
30 ENDPROC
```

Robotics

IRB 4600
Industrial Robot

The IRB 4600 is a pioneer of the sharp robot generation; with enhanced features and new capabilities. The design has been optimized to make it superior for the targeted applications. The IRB 4600 enables more compact manufacturing cells with increased production output and higher quality - and that means improved productivity.

Sharpest accuracy

With the best accuracy in its class, the IRB 4600 can help you increase output with higher process speeds and lower scrap rates, resulting in improved productivity. This is particularly useful in materials handling, dispensing, machining, measuring, assembly and welding applications. In addition, the programming time is minimized since what you program is what you get, and that in the shortest possible cycle time. This is useful in all applications to shorten commissioning times and minimize production stops when new programs or work pieces are introduced.

Shortest cycle times

Thanks to the new compact and optimized design resulting in a low weight, the IRB 4600 can cut the cycle times of the industry benchmark by up to 25%. The maximum acceleration achievable is highest in its class, together with high maximum speeds. The high acceleration is possible to use to avoid obstacles or to follow the path. The benefit is increased production capacity and higher productivity.

Ultra-wide working range

You can position the IRB 4600 in the most favourable way with regard to reach, cycle time and auxiliary equipment. Flexible mounting with floor, tilted, semi-shelf or inverted mounting is very useful when you are simulating the best position for your application.

Compactness

The small footprint, the slim swing base radius around axis 1, the fine elbow behind axis 3, the small lower and upper arms, and the compact wrist all contribute to the most compact robot in its class. With the IRB 4600 you can create your production cell with reduced floorspace by placing the robot closer to the served machines, which also increases your output per m^2 and your productivity.

Best protection available

ABB has the most comprehensive protection program on the market and it will be even further enhanced with the IRB 4600. Foundry Plus includes IP 67, resistant paint, rust-protected mounting flange and protection for molten metal spits on non-moving cables on the rear of the robot and extra protection plates over the floor cable connections on the foot.

Optimize and go sharp

To get the IRB 4600 ready for the targeted applications you have access to high performing workpiece positioners, Track motions, and the motor unit range.

To simulate your production cell to find the optimal position for the robot and program it offline, RobotStudio is available on subscription together with PowerPacs for several applications.

If you would like to learn more about how to use the IRB 4600 in your applications and environments, you can watch simulations on several applications at www.abb.com/robotics

IRB 4600

Main applications

Machine tending, Material handling, Arc welding, Cutting, Dispensing, Assembly, Palletizing and packing, Measuring

Specification

Variants:	Reach	Payload	Armload
IRB 4600-60/2.05	2.05 m	60 kg	20 kg
IRB 4600-45/2.05	2.05 m	45 kg	20 kg
IRB 4600-40/2.55	2.55 m	40 kg	20 kg
IRB 4600-20/2.50	2.51 m	20 kg	11 kg
Number of axes:	6+3 external (up to 36 with MultiMove)		
Protection:	Standard IP67, as option Foundry Plus 2		
Mounting:	Floor, shelf, inverted or tilted		
IRC5 Controller variants:	Single cabinet, Dual cabinet		

Physical

Dimensions robot base:	512 x 676 mm
Robot height: IRB 4600-60/2.05 and IRB 4600-45/2.05	1727 mm
Robot height: IRB 4600-40/2.55 and IRB 4600-20/2.50	1922 mm
Robot weight:	412 to 435 kg

Performance

Position repeatability (RP)	0.05 - 0.06 mm
Path repeatability (RT)	0.13 - 0.46 mm (measured at speed 250 mm/s)

Movement

Axis movements:	Working range:	Maximum speed:
Axis 1	+180° to -180°	175°/s
Axis 2	+150° to -90°	175°/s
Axis 3	+75° to -180°	175°/s
Axis 4	+400° to -400°	250° (20/2.50 has 360°)/s
Axis 5*	+120° to -125°	250° (20/2.50 has 360°)/s
Axis 6	+400° to -400°	360° (20/2.50 has 500°)/s

* Axis 5 for IRB 4600-20/2.50 +120°-120°

Electrical connections

Supply voltage:	200-600 V, 50-60 Hz

Environment

Ambient temperature for mechanical unit:

During operation:	+5° C (41° F) to + 45°C (113°F)
During transportation and storage:	-25° C (-13° F) to +55° C (131° F)
For short periods (max 24 h):	up to +70° C (158° F)
Relative humidity:	Max 95%
Safety:	Double circuits with supervisions, emergency stops and safety functions. 3-position enable device
Emission:	EMC/EMI shielded

Data and dimensions may be changed without notice.

Working range

IRB 4600-60/2.05

IRB 4600-45/2.05

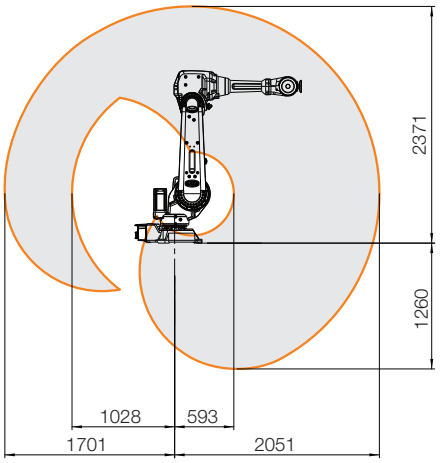

IRB 4600-60/2.05
IRB 4600-45/2.05

IRB 4600-40/2.55

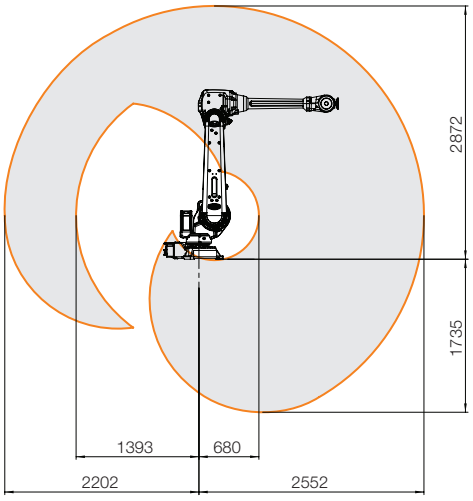

IRB 4600-20/2.50